Contract No. NAS 7-505

(period 5 July 1966 to 28 July 1969)

A STUDY TO ANALYZE THE PERMEATION OF HIGH DENSITY GASES
AND PROPELLANT VAPORS THROUGH SINGLE LAYER TEFLON OR
TEFLON STRUCTURE MATERIALS AND LAMINATIONS
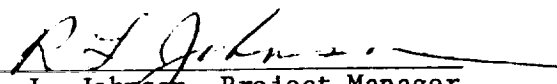
FINAL REPORT

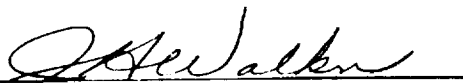15 August 1969   07282-6032-R0-00

Prepared for:

NASA Western Operations Office
Pasadena, California

Prepared by:

R. L. Johnson, Project Manager
Advanced Technology Department

Approved by:

For P. G. Bhuta, Manager
Advanced Technology Department

TRW Systems
One Space Park
Redondo Beach, California

ACKNOWLEDGEMENTS

ABSTRACT

This report contains results of the second phase of a study designed to investigate the leakage rate of pressurant gases and propellant vapors through laminated bladder structures containing an impermeable diffusion barrier as one of the laminates. Under the second phase of the program the formation and growth of vapor bubbles on the bladder surface within the liquid propellant was investigated. The solubility and diffusivity of Helium and Nitrogen pressurant gases in the liquid propellants N_2O_4 and N_2H_4 were also measured and the computer program developed under Phase I was extended to include the effects of gas vapor on the liquid side of the bladder. In addition, the diffusivity of the gases Nitrogen and Helium in the space storable propellant vapors OF_2 and B_2H_6 as well as N_2O_4 and N_2H_4 were determined experimentally.

The results of the study are included in the following report. The design guide which was prepared under Phase I has been updated to include the results of the second phase. The design guide is under separate cover.

TABLE OF CONTENTS

1.0   INTRODUCTION

Under Phase I of this program TRW Systems performed an analytical
and experimental investigation of the leakage rate of pressurant gases
through laminated bladder structures. The pressurant gases considered
were N_2 and He and experimental data was obtained for two types of Teflon,
TFE and FEP. The study consisted of an analytical determination of the
steady state and transient leakage rate of the pressurant gases and
propellant vapors through laminated bladder structures. The laminated
bladder structures considered were assumed to consist of two layers of
Teflon of arbitrary dimensions separated by aluminum foil acting as a
diffusion barrier, which contained holes permitting the leakage of gases
and vapors. One specific case where the holes in the barrier were of
circular shape was solved analytically in a quite rigorous manner. Solu-
tions for other hole shapes , for example rectangular and square, were
obtained in an approximate manner. Finally, a computer program capable of
computing the transient and steady state leakage through holes of arbitrary
shape was developed. The numerical results obtained from the computer
program were found to be in substantial agreement with those obtained
analytically.

Simultaneously with the analytical investigations an experimental
program was carried out to determine the solubility and diffusivity of the
common pressurant gases N_2 and He and the propellant vapor N_2O_4 and N_2H_4
in FEP and TFE type Teflon. Experimental values of the permeability were
obtained for both uni-directional and counter-current flow of gases and N_2O_4
vapor. The experimental results obtained for uni-directional flow were
in good agreement with the values obtained by other investigators but no
previous work was available for comparison with the counter-flow data
obtained.

A laminated bladder structure constructed of 10 mils of TFE and 10
mils of FEP separated by a 1 mil aluminum foil containing fifteen holes
each of diameter 20 mils was obtained in order to experimentally check the
validity of the analytical results. The agreement obtained between the
calculated results and the measured leakage rates was satisfactory when
account was taken of numerous experimental uncertainties.

Although the Phase I effort was successful [except for the measurement of the diffusive properties of N_2H_4 in Teflon] the analytical model assumed was not in strict accordance with the real physical situation. The major simplification adopted under Phase I was the assumption that the body of liquid offered no resistance to the diffusion of pressurant gases through the bladder structure and into the liquid propellant. For some phases of the mission this is a satisfactory assumption. This is particularly true of ground hold and launch where the simultaneous presence of temperature gradients and a large acceleration field insures the presence of strong free convection within the liquid. This results in easy mixing of pressurant gas with propellant and under these circumstances the major resistance to diffusion lies in the bladder structure itself. However, for long space-craft coasts in essentially zero-gravity,thermal convection currents are either absent or are very weak. As a result, the liquid can present a significant resistance to the transfer of pressurant gas from the gas space to within the body of the propellant. The reason for this is as follows. The diffusivity of gases in liquids is about the same order of magnitude as that for gases in Teflon but the body of liquid through which the gas must pass is several orders of magnitude larger than that of the bladder. Consequently, the liquid can in some cases comprise the major resistance to gaseous diffusion. It was therefore decided to investigate the special case where the gas diffuses through the liquid without the aid of free convection. To do this in a meaningful way it was necessary not only to extend the analysis of Phase I to include the presence of the liquid but also to measure the diffusivity of pressurant gases in liquid propellants since this information was not currently available.

Aside from the problem of computing the rate of diffusion of gases through the liquid propellant, there were other questions of immediate interest. It was unclear whether or not the gas goes uniformly into solution in the liquid at the bladder-liquid interface. It appeared that the possibility existed for the formation or nucleation of gas bubbles on the bladder surface. In addition, it was known that a reduction in the total system pressure could result in the evolution of a considerable volume of gas from the liquid propellant and that this gas would, if the free energy of the system was to be minimized, appear on the bladder surface.

Thus, it was desirable to assess the effects of a body of gas on the liquid side of the bladder on the overall leakage rate. In addition, it is important to know the most probable location of any body of gas which forms within the liquid because of its influence on engine start-up problems.

During Phase I the permeation rate of propellants through Teflon was measured using the propellant vapors in contact with the Teflon bladder material. In an actual flight configuration, of course, only liquid propellant is in contact with the bladder. A natural question is, therefore, to what extent do permeation rates measured using vapor apply to cases where the liquid is in contact with the bladder surface.

Finally, in accordance with NASA's interest in high energy mild cryogenic space storable propellants it was desirable to make the first step in extending the program so the results would apply to the propellant combination OF_2-B_2H_6. Accordingly, it was decided to measure the diffusion coefficients of the space storable propellant vapors OF_2 and B_2H_6 for the case of binary diffusion into the gases N_2 and He.

All the objectives of the program, as outlined above, have been met. The analytical results of Phase I have been extended to include the presence of liquid propellant and the computer program developed under Phase I has been appropriately modified. The binary diffusion coefficients of OF_2 and B_2H_6 vapor in He and N_2 have been measured and the solubility and diffusivity of the pressurant gases N_2 and He in the liquid propellants N_2O_4 and N_2H_4 has been determined experimentally.

Early in this phase of the program experiments using glass apparatus were performed to clarify the mechanics by which pressurant gas is transferred from the bladder to the liquid propellant. It was found that although some of the gas goes directly into solution in the liquid, the remainder of the gas enters the liquid from gas bubbles which are nucleated on the surface of the bladder. The rate of growth of these bubbles has been calculated and appears to be in reasonable agreement with that observed.

Again, a laminated bladder structure containing holes of known size in the diffusion barrier was obtained and experiments carried out to obtain data for comparison with the analysis. The effect of bodies of gas in the liquid propellant on the overall leakage rate has been assessed and the

position of these bodies during spacecraft coast determined. Finally, a literature search was carried out in order to assess the probable error in permeation rates measured using vapor rather than liquid. The results of all this work are reported in detail in the sections which follow.

2.0 PRELIMINARY EXPERIMENTS AND ANALYSIS

2.1 Visual Observations of Bubble Formation and Growth

The objective of these experiments was to determine whether or not gas bubbles form on the liquid side of a Teflon bladder separating liquid propellant and if so to determine the growth rate of these bubbles. Two such samples were studied, the first being a laminate of 5 mils of TFE Teflon and 5 mils of FEP Teflon and the second being a 5 mil FEP Teflon - 1 mil aluminum foil - 5 mil FEP Teflon sandwich with a pattern of fifteen 20 mil diameter holes in the aluminum foil. All tests were conducted using hydrazine as the liquid propellant and He as the pressurant gas.

Bubble growth tests were performed with the TFE-FEP laminate to determine the bubble growth rate and its dependence on tank pressurization and the presence of liquid propellant on the pressurant side of the bladder. Tests were conducted with total system pressures of 1 atm., 2 atm. and for two cases where the pressure was held at 1 atm. for many hours and then increased suddenly to 2 atm. and held for a further period of time. In one of the two latter cases the pressurant gas (He) side of the test cell contained 15 ml of liquid hydrazine while in the remaining case the pressurant gas side contained He only. The tests involving the step change in pressure from 1 to 2 atm. were conducted to determine the response of existing gas bubbles on the liquid side of the bladder to this change. The test with the liquid hydrazine present on the gas side was performed to determine if the bubble growth rate was effected by the presence of hydrazine vapor on the gas side of the bladder.

In later tests the FEP-Aℓ-FEP bladder sample, as shown schematically in Figure 2.1-1, was installed in the bubble growth apparatus and tests conducted at 1 and 2 atm. for several days.

The apparatus utilized for observation of gas bubble growth on bladder samples is shown in Figures 2.1-2 and 2.1-3. It was designed specifically to facilitate measurement of bubble growth at the bladder/ propellant interface, resulting from pressurant gas diffusion through the bladder. As can be seen in the photographs, the apparatus is basically a standard Pyrex glass pipe joint, equipped with inlet and outlet lines for evacuation, pressurization and liquid propellant transfer, an optical window at each end of the cell, and an absolute pressure gage on the gas pressurant
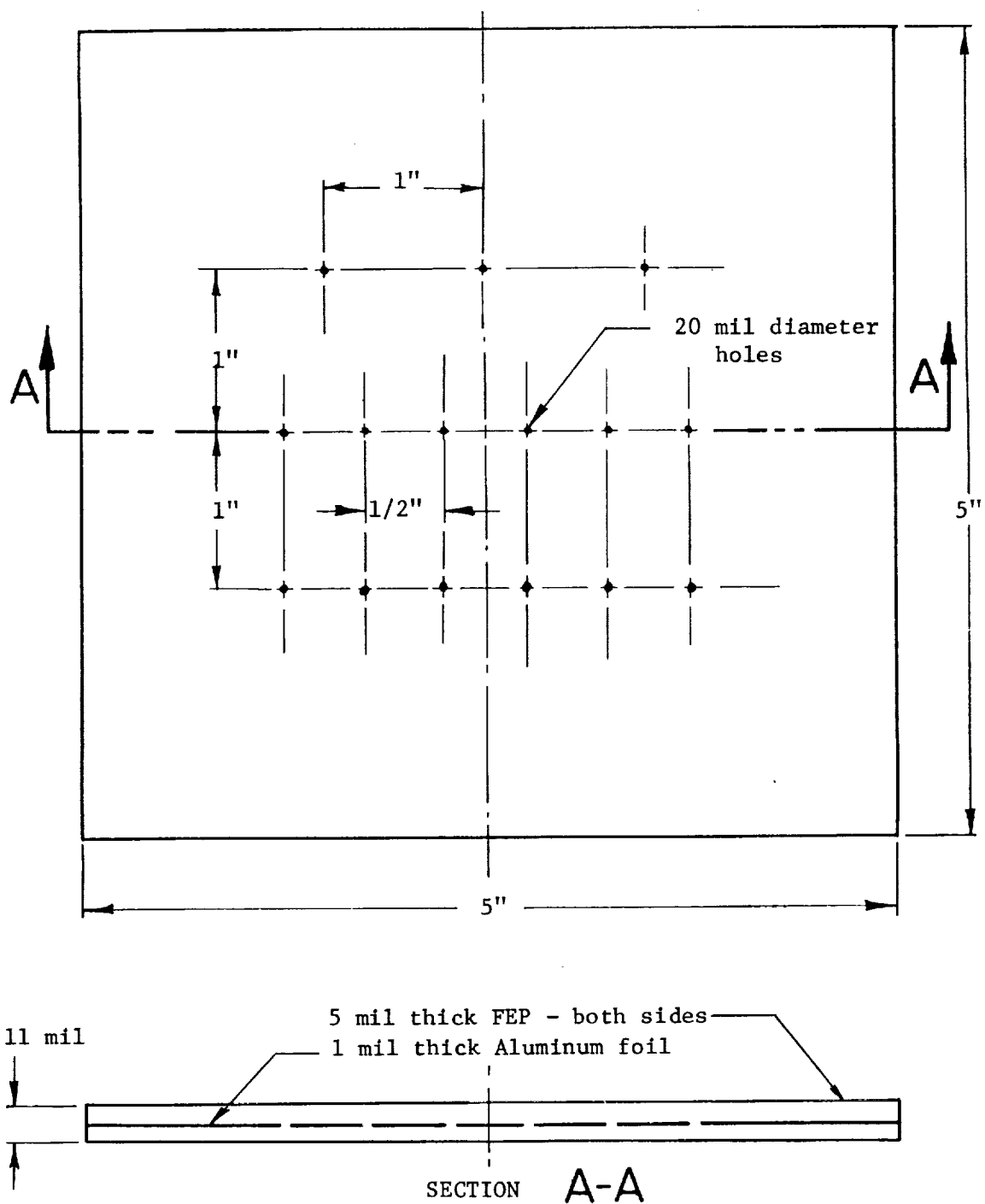
Figure 2.1-1 Specially Prepared FEP-Al-FEP Laminate With Holes
in the Aluminum Foil.

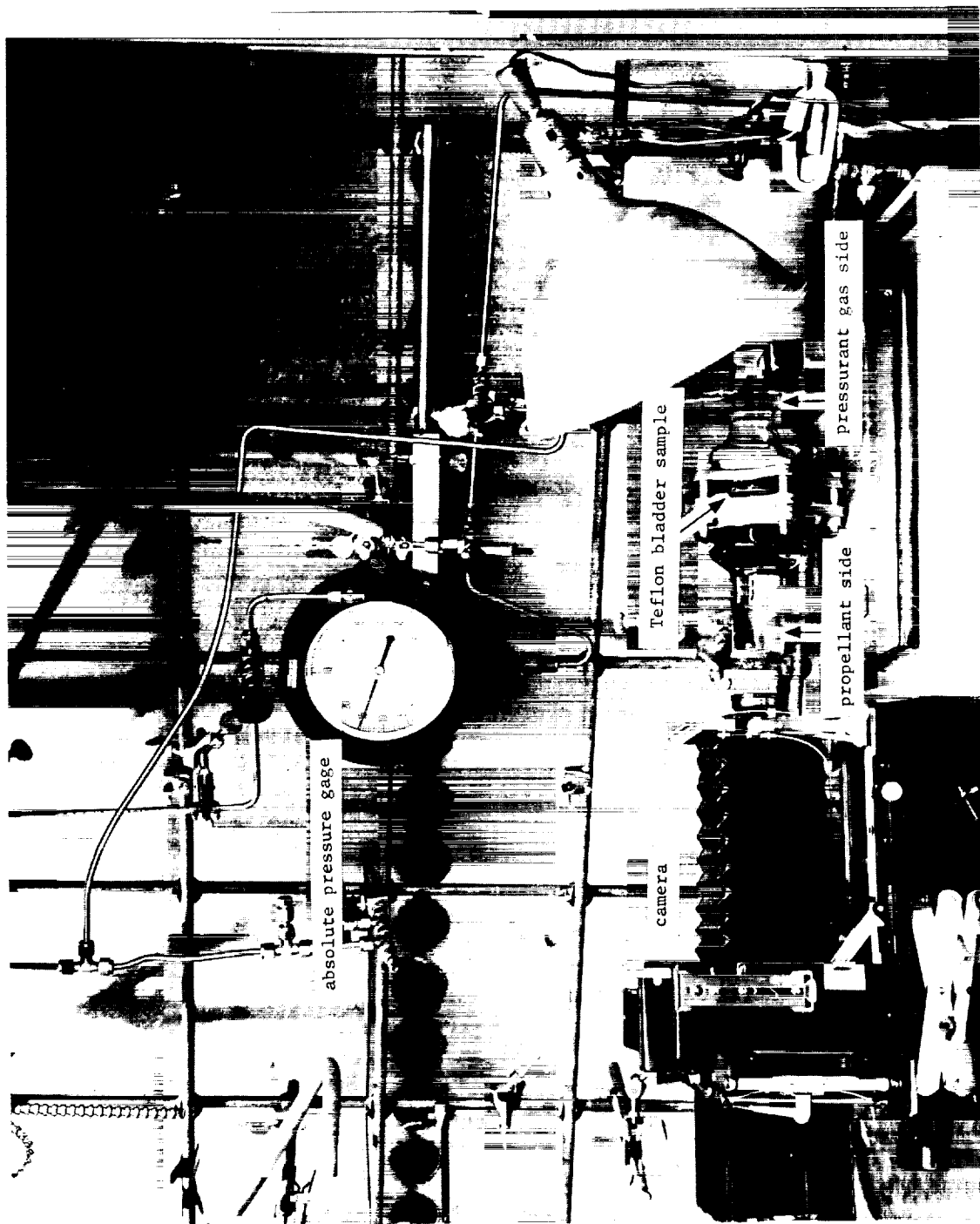Figure 2.1-2 Bladder Sample Bubble Growth Test Cell

Figure 2.1-3 Bubble Growth Test Cell With Auxiliary Equipment

The image contains the following labels:
- absolute pressure gage
- Teflon bladder sample
- pressurant gas side
- propellant side
- camera

side. The volume capacities of both liquid and gas sides are nearly identical and are approximately 350 ml.

The test specimen/apparatus configuration as shown in Figure 2.1-3 evolved during the course of the study and was the result of corrective design modifications to solve and/or eliminate specific experimental difficulties. Problems identified and modifications implemented include:

o   Unrelieved stresses, especially in the area of metal to glass joints, caused excessive breakage. This problem was remedied by incorporating flexible stainless steel lines at the interfaces and modifying inlet and outlet lines.

o   Measurement of bubble sizes as a function of time utilizing the cathetometer was very time-consuming and subject to error because of realignment problems. This situation was alleviated by the use of a Polaroid camera which was "precalibrated" by determining the ratio of photographic image size to the bubble size measured with a cathetometer.

o   Other corrective measures included prevention of bladder distention, shortening the path length from the optical window to the bladder, and the design and construction of a special degassing and transfer manifold.

The procedure which evolved from these modifications and which was used for the tests reported here is as follows. Propellant was added to the propellant evacuation reservoir attached to the transfer manifold as shown in Figure 2.1-4. With the lower reservoir stopcock closed and the bubble growth test cell needle valve open to the vacuum pump, the gas and liquid side of the cell as well as the bladder sample were evacuated, typically for 24 hours. The propellant was concurrently degassed by pumping down the propellant evacuation reservoir to the vapor pressure of the hydrazine then closing the stopcocks to prevent distillation of the hydrazine. The reservoir was periodically re-evacuated to the vapor pressure of hydrazine to pump out gases evolved from solution. After evacutation, the propellant was transferred to the propellant side of the test cell by closing the vacuum stopcocks and opening the lower reservoir stopcock. Transfer proceeded via gravity feed. The liquid side needle valve was closed and the pressurant side pressurized with He to the level required for the particular test. During the filling process the bladder sample became distended (1/8" to 1/4")
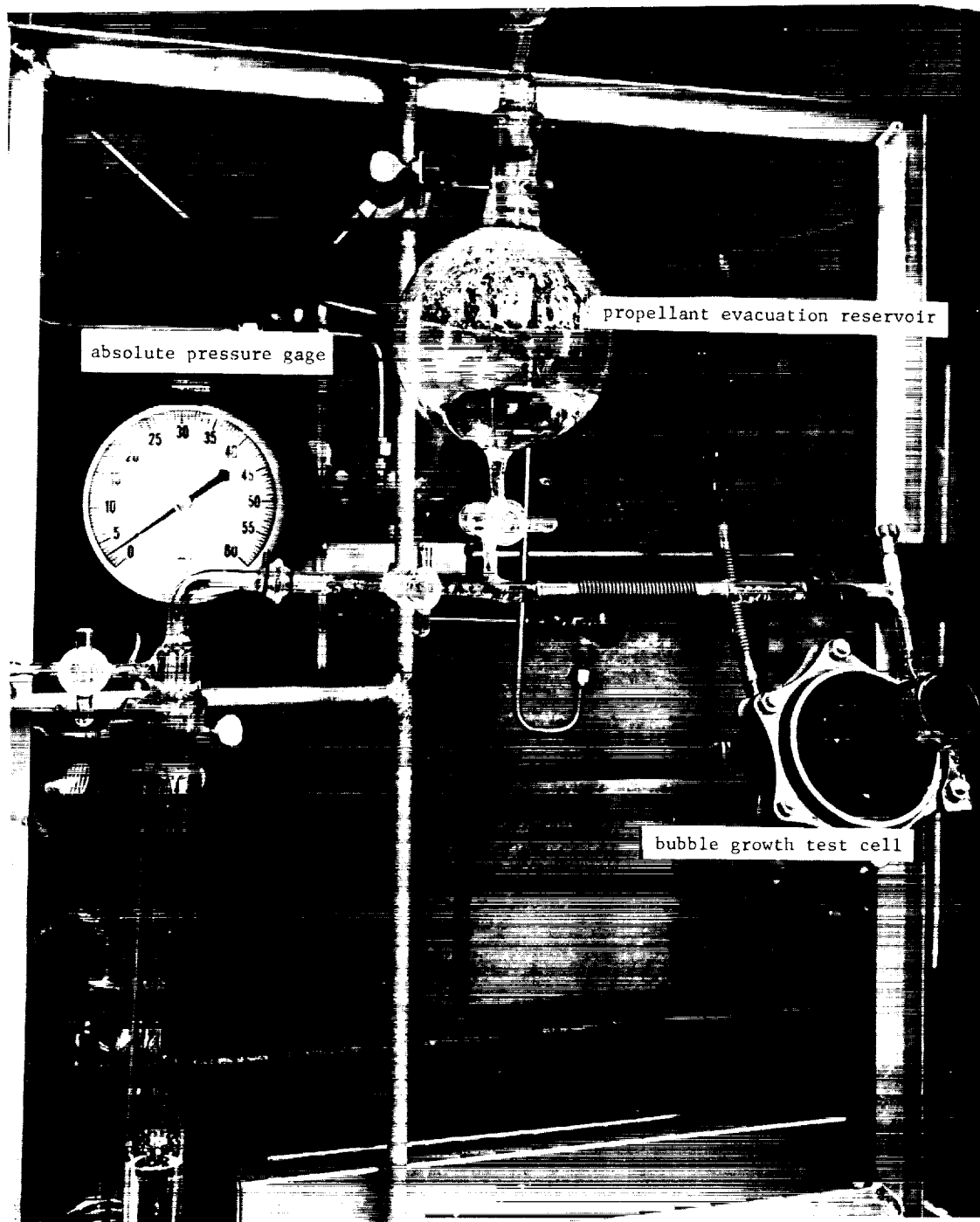
Figure 2.1-4   Propellant Evacuation Reservoir
and Transfer Manifold

to the gas side and had to be corrected to the neutral position so that the experiment is performed with the bladder in a relatively stress free condition (to minimize artifacts in the data arising from creation of stress fissures or enlargement of existing faults). This was accomplished by opening the liquid side needle valve and allowing liquid to drain out while observing the position of the bladder sample. When the sample was observed to be no longer distended, the needle valve was closed.

The loaded and pressurized test cell was then disconnected from the transfer manifold and positioned in front of the calibrated Polaroid camera for photographic recording of bubble growth. Pre-calibration was accomplished during a preliminary experiment by measuring the size of bubbles with the cathetometer and then photographing the bubble in rapid sequence, alternating between measuring and photographing. All photographs in this study were taken with the same lens combination (the normal 135 mm objective and a +2 closeup lens) and with the same lens-to-film plane distance.

In the experiment directed at evaluation of the effect of fuel vapor on the pressurant side, 15 milliliters of hydrazine were added to the pressurant side of the cell through the pressurant inlet line prior to degassing the cell. The cell and propellant reservoir were then evacuated as described above. However, because of the presence of liquid fuel in the cell, it was not possible to evacuate for the lengthy period used in the dry cell experiments.

Four tests were conducted, numbered from 1 to 4, with the 10 mil FEP-TFE laminate, and are presented in Figures 2.1-5 and 2.1-6. In Figure 2.1-5 are plotted the growth rates of representative bubbles for each test normalized by dividing by the initial radius observed at the start of the test. Tests 1 and 2 were each run for about six hours. The system pressure for Test 1 was held at 1 atm. and for Test 2 it was maintained at 2 atm. for the duration of the test. Tests 3 and 4 were conducted over a much longer period of time, about 24 and 29 hours respectively. The first seven hours of these tests are plotted in Figure 2.1-5 for comparison with Tests 1 and 2 while the dimensional results of the complete test period are presented in Figure 2.1-6. Also shown in Figure 2.1-5 are the bubble growth rates using Equation 2.2-12 of the next section with various values of the

permeation coefficient of He in TFE Teflon, which is less than that in FEP Teflon. the value of 10^{-7} cc(STP) cm/cm^2 sec atm was found experimentally during Phase I of the present study. Also shown are results of Equation (2.2.12) using a permeability coefficient of 10^{-6} and 10^{-5} cc(STP) cm/cm^2 sec atm. The discrepancy between the experimentally observed growth rates and that calculated using Equation (2.2.12) and the value of the permeability coefficient of 10^{-7} could be due to a number of factors. First of all, discrepancies in measured values of permeabilities of an order of magnitude are not uncommon (Reference 1). Secondly, the bladder sample used for the bubble growth tests was not the same as that used for the permeability tests and thirdly, decomposition of the hydrazine into NH_3, caused by impurities on the surface of the Teflon could add to the bubble volume causing a growth rate much greater than that predicted by Equation (2.2.12) which accounts for the growth due to the permeation of pressurant gas only.

As can be seen from Figure 2.1-6, the increase in total system pressure from 1 atm to 2 atm caused an immediate decrease in bubble diameter followed by an increase in bubble diameter within a very short time after the pressure increase to 2 atm. Using the results of Phase I (Reference 1) the expected transient through a 10 mil thick bladder is on the order of minutes. A resumption of bubble growth shortly after pressurization is therefore expected. It is also seen from Figure 2.1-6 that the presence of hydrazine vapor on the pressurant gas side did cause a decrease in bubble growth rate.

Representative photographs of the bladder surface at different times during the various tests are presented in Figures 2.1-7 through 2.1-10.

After the above experiments had been completed, the FEP-Aℓ-FEP laminate was placed in the bubble growth test cell. Two bubble growth tests were conducted with this arrangement. All tests were performed with He only on the gas side of the cell. In Test Number 1 the total system pressure of 1 atm was held for a period of 5 days. During this time no gas bubbles were observed on the hydrazine side of the bladder. Figure 2.1-11 contains two photographs of the liquid side of the bladder, one taken at the beginning of the test and one taken at the end of the five day test period. Test Number 2 was conducted somewhat later than the first and it was found that the FEP Teflon had become detached from the aluminum foil, particularly in the area of the holes in the foil. The cell was pressurized to 1 atm with

He and held at this pressure for 67.5 hours, at which time the pressure was increased to 2 atm and maintained for the remainder of the test for 24 hours. At no time during the 91.5 hour test did bubbles appear on the bladder surface. The photographs of Figure 2.1-12 show the liquid side of the bladder at the beginning of the test, when the pressure was increased to 2 atm and at the end of the test. Since the loading procedure was the same as for the TFE-FEP laminate tests, the absence of bubbles in the FEP-Aℓ-FEP laminate test is thought to be due to a difference in surface condition between this bladder sample and the TFE-FEP laminate sample. Under magnification the surface of the FEP-Aℓ-FEP laminate appears much more smooth than the TFE-FEP laminate surface. This would indicate that there are less surface roughness cavities which could act as nucleation sites.
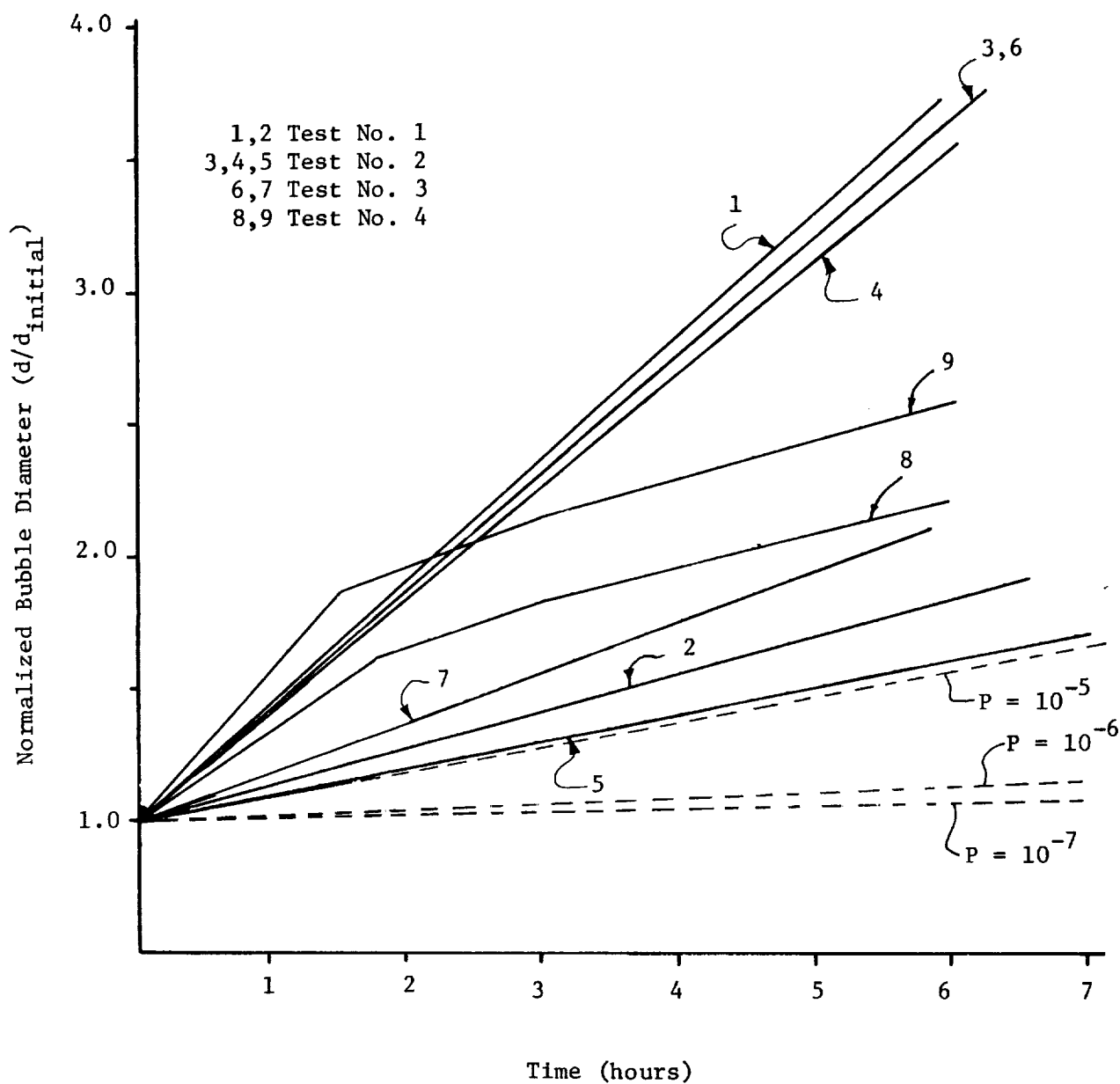
Figure 2.1-5 Normalized Bubble Growth Rates
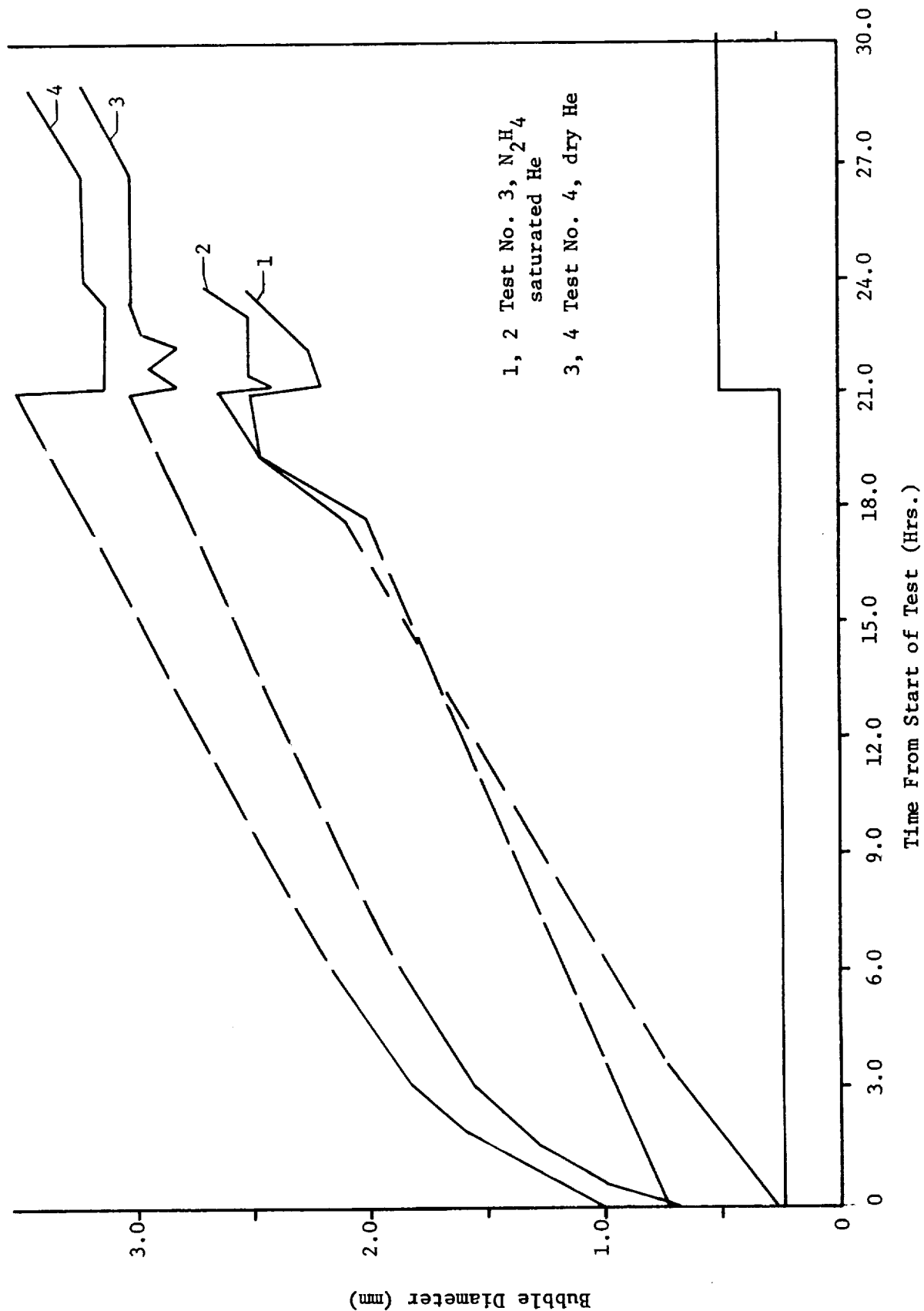
Figure 2.1-6   Bubble Growth Results for Tests 3 and 4
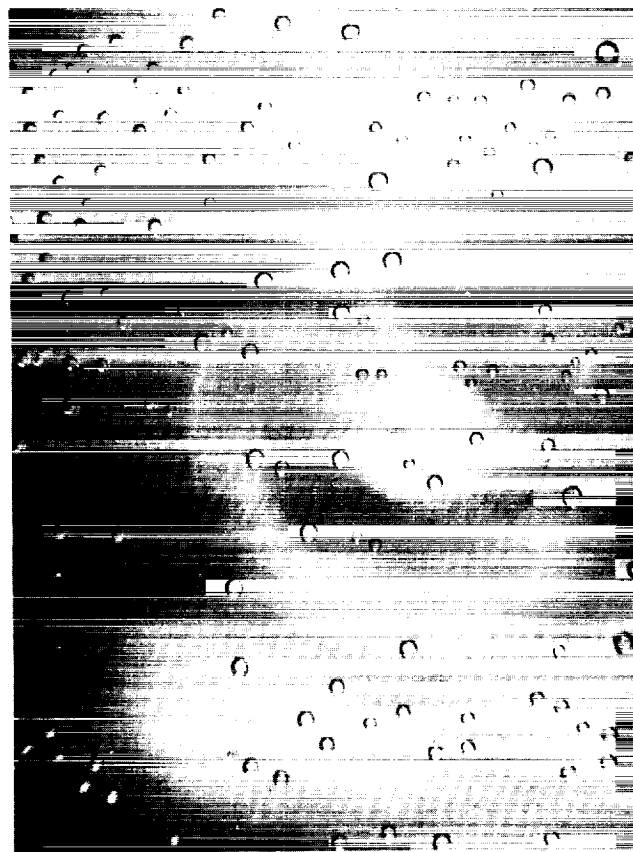
(a) 20 Minutes After Start of Test
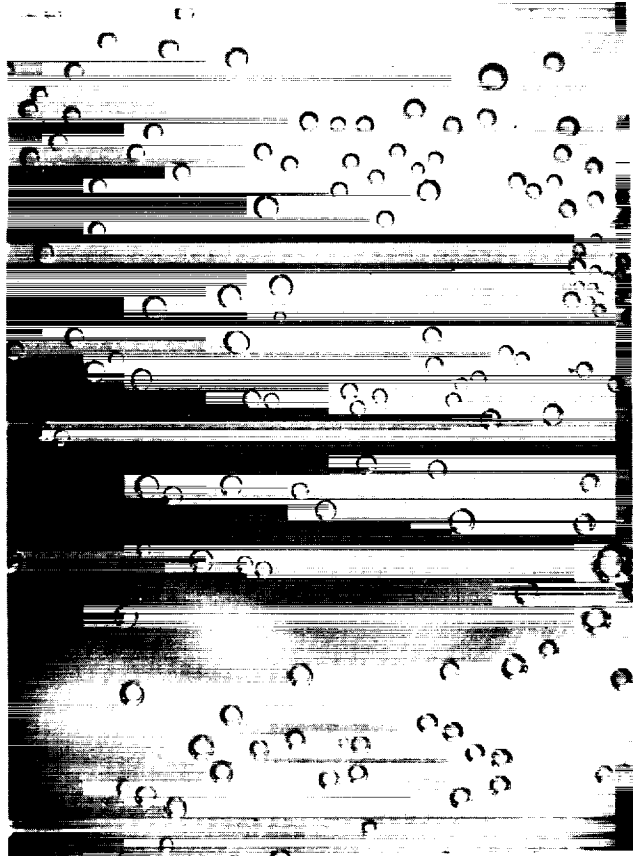
(b) 2 Hours After Start of Test

Figure 2.1-7   Bubble Growth Photographs for Test 1
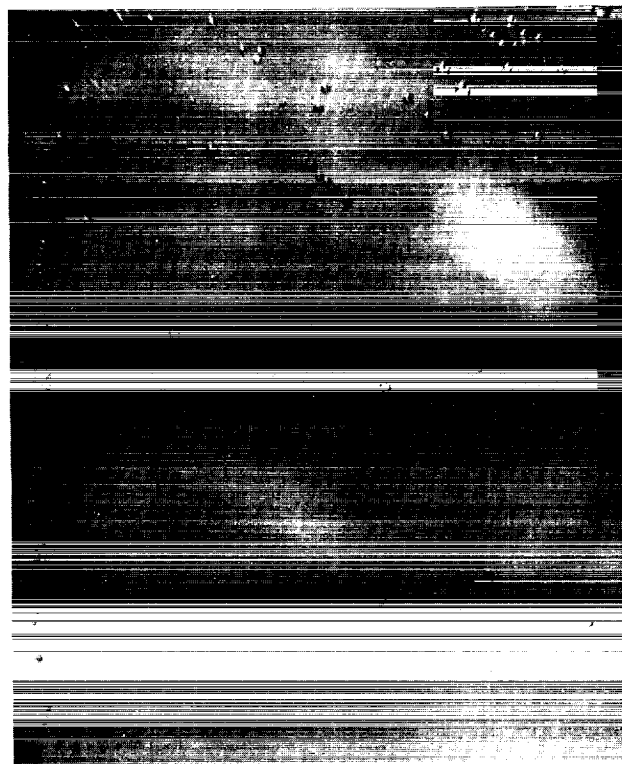
(a) 20 Minutes After Start of Test
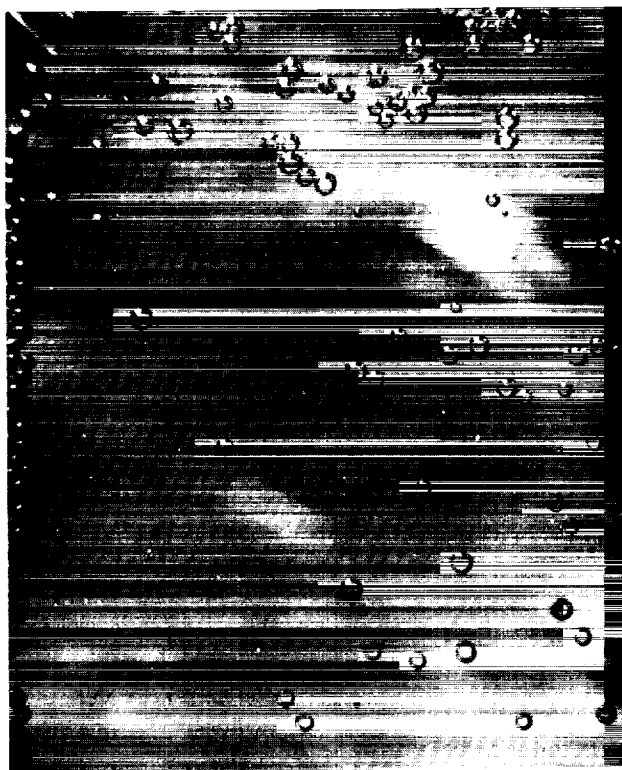
(b) 3 Hours After Start of Test

Figure 2.1-8 Bubble Growth Photographs for Test 2

2-13
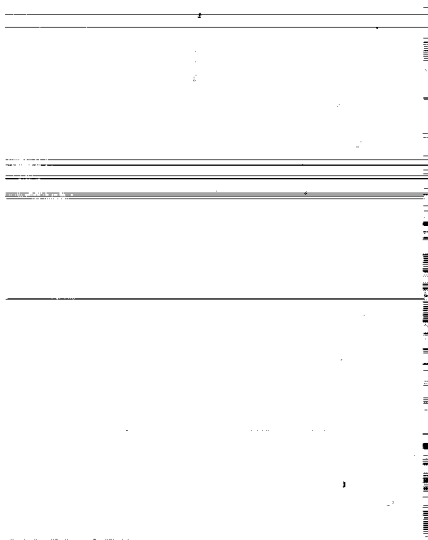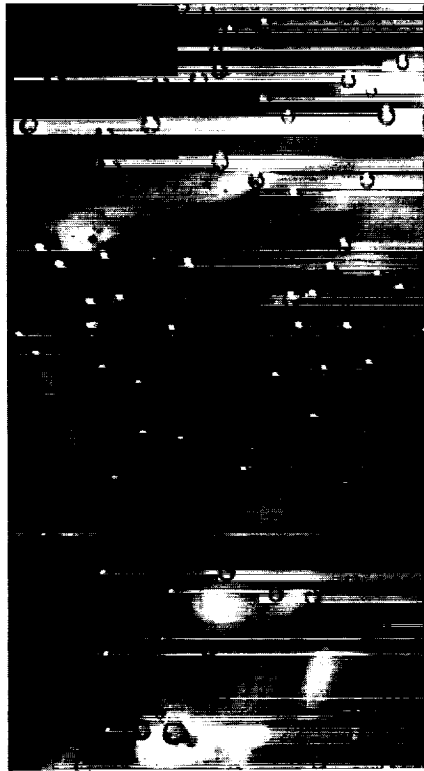
(b) Four Hours After Start of Test

(d) Three Minutes After Pressure Increase From 1 to 2 atm.

(a) Start of Test

(c) 22 Hours After Start of Test

Figure 2.1-9 Bubble Growth Photographs for Test 3

2-14
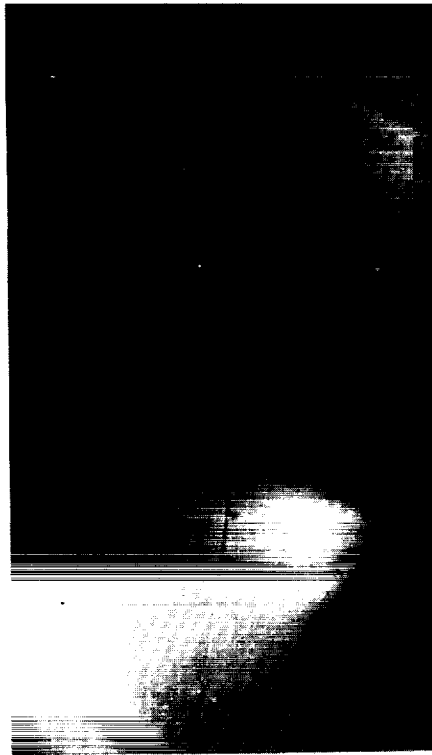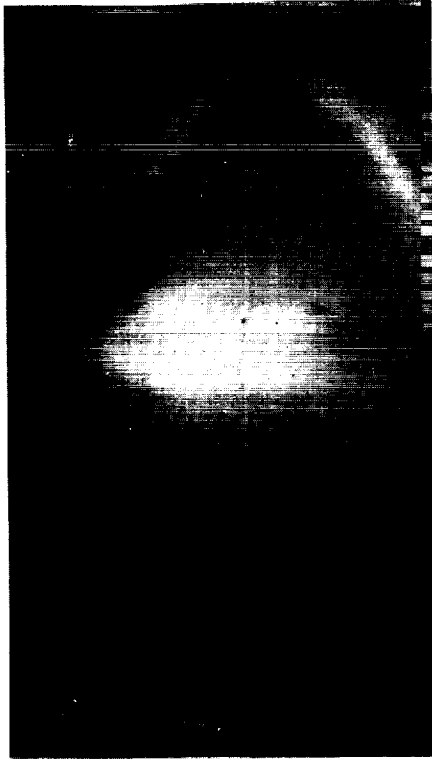
(b) 3-1/2 Hours After Start of Test

(d) One Minute After Pressure Increase From 1 to 2 atm.
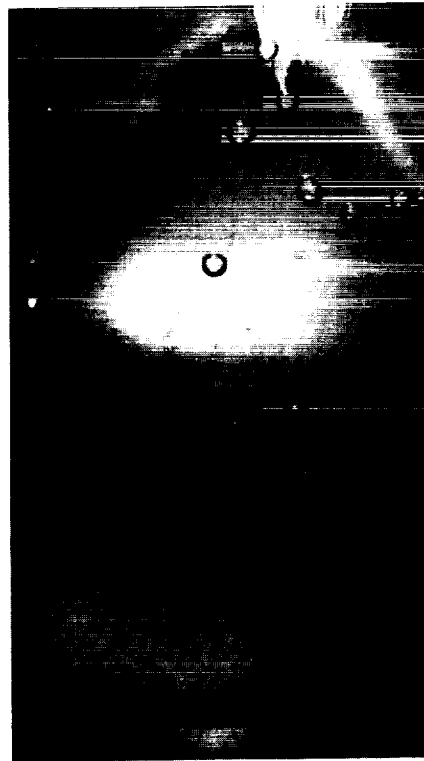
(a) Start of Test

(c) 21 Hours After Start of Test

Figure 2.1-10   Bubble Growth Photographs for Test 4

(a) Start of Test

(b) 5 Days After Start of Test

Figure 2.1-11 Bladder Photographs for FEP-Al-FEP Test 1

(c) 24 Hours After Pressure Increase to 2 Atm.

(b) 67 Hours After Start of Test, Pressure Increased to 2 Atm.

Figure 2.1-12   Bladder Photographs for FEP-Al-FEP Test 2

2.2   Comparison of Observed with Calculated Growth Rates

The experiments reported in Section 2.1 above indicate that gas bubbles are formed on the liquid side of the bladder within a very short time after loading the test apparatus with hydrazine. These bubbles grow with time and ultimately break away from the bladder surface and rise to the top of the apparatus. It appears that the mechanism of bubble formation and growth could be somewhat as follows.

The surface structure of Teflon on a micronic scale can be quite rough containing micro voids and other irregularities which act as bubble nucleation sites. When the liquid is loaded, small quantities of gas and/or propellant vapor are trapped in the micropores by surface tension. Gas leaking through the bladder from the gas side adds to the gas already present in these irregularities resulting in the growth of a bubble. The bubbles grow slowly being limited in this regard by the leakage rate through the bladder material and the rate of leakage of the gas from the bubble into the liquid. In the paragraphs below we present a simplified analysis of the phenomenon which seems to substantiate the observations.

Consider the system shown in Figure 2.2-1. The gas bubble is assumed at all times during its growth to have the shape of a segment of a sphere with a constant contact angle, θ, consistent with the particular propellant and bladder material. In the following development, the radius of the bubble contact area on the bladder surface, r, will be used since this is the dimension observed experimentally. Also, in the following discussion the subscripts g and v refer to the gas spaces on the outside of the bladder and inside of the gas bubble, respectively.
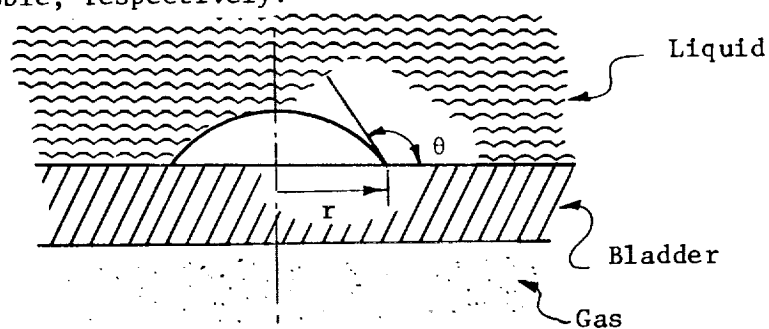
Figure 2.2-1   Bubble Growth Model

Letting p be the total system pressure and taking account of the surface tension, σ, we have

$$p_g^2 + p_v^2 = p + \frac{2\sigma}{r} \sin\theta \qquad (2.2.1)$$

$$p_g^1 + p_v^1 = p \qquad (2.2.2)$$

where p_g^1 = partial pressure of gas on gas side

p_g^2 = partial pressure of gas on liquid side (within bubble)

p_g^1 = partial pressure of vapor on gas side

p_v^2 = partial pressure of vapor on liquid side (within bubble)

r = instantaneous bubble radius on the bladder surface (cf. Figure 2.2-1)

Subtracting Equation 2.2.1 from 2.2.2 we obtain

$$p_g^1 - p_g^2 = p_v^2 - p_v^1 - \frac{2\sigma}{r} \sin\theta \qquad (2.2.3)$$

Initially at least, p_v^1 is small since the permeation rate for propellant vapor is small compared to that for the gas. Thus,

$$p_g^1 - p_g^2 = p_v^2 - \frac{2\sigma}{r} \sin\theta \qquad (2.2.4)$$

is the driving partial pressure difference for the flow of pressurant gas from the gas space across the bladder into the bubble.

As a good first approximation we may assume that only gas which flows through the area of the bladder covered by the bubble adds to the bubble volume. In addition, we can estimate the leakage rate across the bladder by its steady state value. This is a reasonable assumption since the diffusion coefficients of gas in the bladder and in the liquid propellant

are of the same order of magnitude, while the thickness of the bladder is several orders of magnitude less than a characteristic dimension of the liquid volume. Thus, the characteristic time for flow through the bladder is much smaller than that for diffusion in the liquid. The leakage rate, j_i, through the bladder into the bubble is then

$$j_i = k_s \left(p_v^2 - \frac{2\sigma}{r} \sin \theta \right) \frac{\rho_s D_s}{\ell_s} \pi r^2 \qquad (2.2.5)$$

where ρ_s is the density, D_s the diffusivity, k_s the solubility, and ℓ_s the thickness of the bladder material. If we approximate the leakage rate of gas from the bubble by that obtained for the transient diffusion of gas into a semi-infinite medium, then the rate of departure of gas from the bubble is given by

$$j_o = \frac{\rho_\ell D_\ell k_\ell}{\sqrt{\pi D_\ell t}} \left(p - p_v^2 + \frac{2\sigma}{r} \sin \theta \right) 2\pi r^2 \frac{(1 + \cos \theta)}{\sin^2 \theta} \qquad (2.2.6)$$

Equating the difference between equations 2.2.5 and 2.2.6 to the time rate of change of the mass contained by the bubble we have

$$\frac{d}{dt} \left(\frac{1}{3} \rho_g \frac{r^3}{\sin^3 \theta} (1+\cos \theta)^2 (2-\cos \theta) \right) = k_s \left(p_v^2 - \frac{2\sigma}{r} \sin \theta \right) \frac{D_s \rho_s}{\ell_s} \pi r^2$$

$$- \frac{\rho_\ell D_\ell k_\ell}{\sqrt{\pi D_\ell t}} \left(p - p_v^2 + \frac{2\sigma}{r} \sin \theta \right) 2\pi r^2 \frac{(1+\cos \theta)}{\sin^2 \theta} \qquad (2.2.7)$$

which is valid for values of time not too close to zero.

Upon simplifying and rearranging (2.2.7) becomes

$$\frac{dr}{dt} = \frac{K_s D_s \rho_s \sin^3 \theta}{\ell_s \rho_g (1+\cos \theta)^2 (2-\cos \theta)} \left(p_v^2 - \frac{2\sigma}{r} \sin \theta \right)$$

$$- \frac{\rho_\ell D_\ell K_\ell}{\rho_g \sqrt{\pi D_\ell t} (1+\cos \theta)(2-\cos \theta)(\sin \theta)} \left(p - p_v^2 + \frac{2\sigma}{r} \sin \theta \right) \qquad (2.2.8)$$

A number of pertinent observations can be made from this relation. First of all, for a total system pressure, p, greater than the propellant vapor pressure, the above relation indicates that there is a minimum radius given by

$$p_v^2 = \frac{2\sigma \sin \theta}{r_{min}} \qquad (2.2.9)$$

Bubbles with radii less than r_{min} will collapse while those with radii above r_{min} can grow.

In order to estimate r_{min} from Equation (2.2.9), a value for the solid-liquid contact angle, θ, is required. For the purposes of this model, an equivalent contact angle can be obtained by considering a force balance on the bubble between surface tension and bouyancy and using the experimentally observed critical bubble radius to determine an equivalent contact angle from the resulting expression. Equating surface tension and bouyancy forces on the bubble yields the following relationship for the critical bubble radius at which the bubble will leave the bladder surface under the influence of a non-zero gravity field, βg,

$$r_{critical}^2 = \frac{6\sigma \sin^4 \theta}{(1 + \cos \theta)^2 (2 - \cos \theta) \, \rho_\ell \beta g} \qquad (2.2.10)$$

For the purposes of this bubble growth model an equivalent solid-liquid contact angle can be obtained from Equation (2.2.10) using the experimentally observed value of the critical bubble radius. This value was found in the series of preliminary experiments reported in Section 2.1 to be about 1/8" or about 0.31 cm. Inserting this value in Equation (2.2.10) yields an equivalent contact angle, θ, of 65°.

Substituting this value of θ into Equation (2.2.9) yields, for hydrazine at room temperature, a minimum radius of 3.6×10^{-3} inches and for nitrogen tetroxide at room temperature a minimum radius of 2.5×10^{-5} inches. These results indicate that bubble formation is much easier in the oxidizer N_2O_4.

2-21

The second observation to be made from Equation (2.2.8) is that, by inserting the values of the various diffusive properties in Equation (2.2.8), the relative sizes of the two terms on the right hand side can be obtained for times not close to zero and radii of the order observed in the laboratory, about 10 mils. It is found in this way that at a time of 10 seconds, the second term is about two orders of magnitude less than the first term. Since the major portion of the experimentally observable growth takes place over a period of hours, this term can be neglected. The governing expression is then

$$\frac{dr}{dt} = \frac{K_s D_s \rho_s \sin^3 \theta}{\ell_s \rho_g (1+\cos \theta)^2 (2-\cos \theta)} \left(p_v^2 - \frac{2\sigma}{r} \sin \theta \right) . \tag{2.2.11}$$

which is of simple form and can be integrated directly. The result is

$$t = \frac{\ell_s \rho_g (1+\cos \theta)^2 (2-\cos \theta)}{K_s D_s \rho_s p_v^2 \sin^3 \theta} \left[(r-r_i) + C \ln \left[\frac{r-C}{r_i-C} \right] \right] \tag{2.2.12}$$

where $C = \dfrac{2\sigma \sin \theta}{p_v^2}$

Equation (2.2.12) above, together with the equivalent contact angle found from Equation (2.2.10) for hydrazine and the experimentally observed initial radius, can be used to calculate a bubble growth rate for comparison with the rates observed in the laboratory. This was done for an equivalent contact angle of 65°, an initial bubble radius of 0.5 mm and the permeation data found during Phase I of this program. The resulting curve is shown in Figure 2.1-5 of Section 2.1 and is marked "P =10^{-7}", the value of the permeability constant in units of cc(STP) cm/cm^2 sec atm found experimentally during Phase I. Since order of magnitude variations in permeation data are not uncommon, Equation (2.2.12) is also plotted using values of the permeability of 10^{-6} and 10^{-5} cc(STP) cm/cm^2 sec atm. The disagreement with experimentally observed growth rates could be due in part to the fact that the bladder sample used for the bubble growth tests was not the same as that used for the collection of the permeation data of Phase I. Decomposition of hydrazine, generating NH_3 in the test cell, could also be

contributing to the bubble growth causing it to be greater than that predicted assuming pure diffusion as in Equation (2.2.12). Extensive experiments in which the same bladder sample is used for the permeation and bubble growth tests and in which the bubbles formed on the bladder are analyzed for their chemical constituents are necessary to assess the accuracy with which Equation (2.2.12) can predict bubble growth.

2.3   Effect of System Pressure Changes on Size of Gas Bubbles

The experiments described in Section 2.1 above indicate that, under certain conditions gas and vapor bubbles can be formed on the liquid side of a bladder separating a liquid propellant and pressurant gas. Of vital importance to a given mission would be a knowledge of the response of such a gas bubble or pocket to an increase in pressurant gas pressure, as would be the case for a spacecraft whose bladder expulsion system is actuated by pressurization following a long low-g coast.

The response may be analyzed by considering the following configuration. Since the permeation of gas and vapor is not a strong function of the system geometry, we consider the one-dimensional problem shown schematically in Figure 2.3-1.
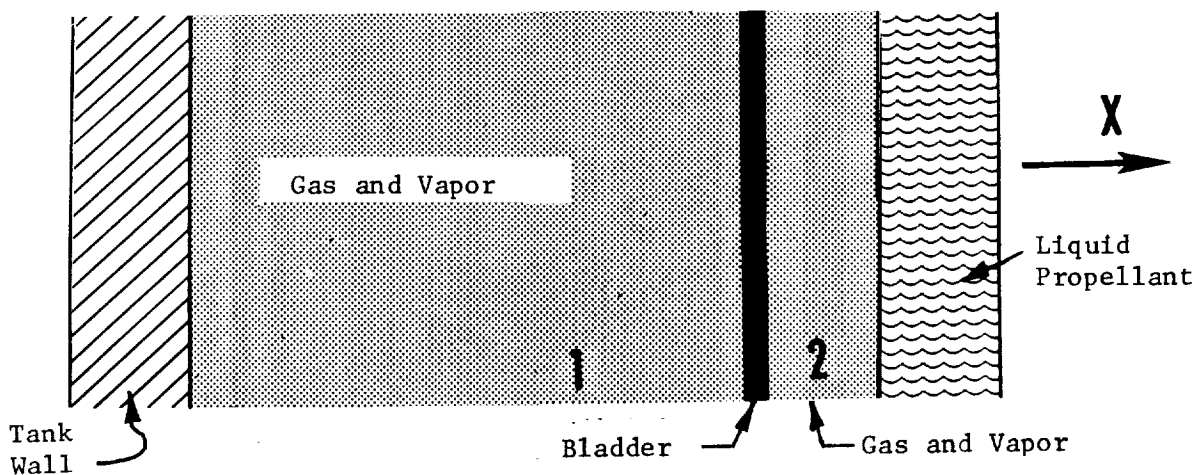
Figure 2.3-1   Illustrating Geometry for Vapor Space Collapse

Recall that the diffusive constant in the bladder is of the same order of magnitude as that in the liquid. Since the thickness of the liquid volume is typically three orders of magnitude greater than the bladder thickness, the response of the gas and vapor volume behind the bladder to diffusive processes following a gross change in system pressure or temperature can certainly be estimated by neglecting the transient diffusive flow through the bladder. Assuming further that the bladder responds (without friction) instantaneously to any pressure changes and that the partial pressure of propellant vapor is kept constant in the space behind the bladder by evaporation, the analysis may be conducted in two parts. For the first part, the

2-24

bladder is moved to its new location required by mechanical equilibrium
with no diffusion taking place. Subsequent bladder motion from this
mechanical equilibrium position due to the diffusion of pressurant gas and
propellant vapor is then computed using as initial conditions the partial
pressure differences present after mechanical equilibrium is reached.
Incompressible liquid propellant and the perfect gas law are assumed.

The complete development is included in Appendix 7.1. The result,
expressing the final volume of gas in vapor space 1 (refer to Figure 2.3-1)
after the complete process of pressurization and subsequent permeation of
gas and propellant vapor is given below. In that expression the subscripts
g, v, and ℓ refer to the pressurant gas, propellant vapor and liquid; sub-
scripts i and f refer to states before and after the bladder moves by
pressurization (but before it moves due to the permeation of pressurant
gas and propellant vapor) and superscripts 1 and 2 refer to the gas-vapor
spaces exterior and interior to the bladder. The result is:

$$V^1(\infty) = \frac{\left[(1-W)V + WV_i^1\right]\left[NP_f + (1-N)\left(\dfrac{P_v^2}{(1-W)\dfrac{V}{V_i^1} + W}\right)\right]}{P_v^2 + NP_f\left[\dfrac{1 + k_\ell \dfrac{V_\ell}{V} RT\left(\dfrac{P_i - P_v^2}{P_f}\right)}{1 + k_\ell \dfrac{V_\ell}{V} RT}\right]} \qquad (2.3.1)$$

where $W = \dfrac{P_i - P_v^2}{P_f - P_v^2}$, with P_i = initial total system pressure, P_f = final
total system pressure, P_v^2 = propellant vapor pressure

$N = \dfrac{\overline{P}_v}{\overline{P}_g}$, with $\overline{P}_v$, $\overline{P}_g$ = permeabilities of vapor and pressurant gas
through the bladder.

k_ℓ = solubility of pressurant gas in liquid propellant

V_ℓ = volume of liquid propellant

V = total volume of gas spaces on either side of the bladder (constant)

R = universal gas constant

T = absolute temperature

Solutions to the above equations for nitrogen tetroxide at 300°K using the diffusivity and permeation data collected under both phases of this contract are presented in the table below for an initial total pressure of 3.0 atm, a liquid N_2O_4 volume of 200 liters and a combined gas volume 30 liters.

TABLE 2.3-1

	P_f Final Total System Pressure (atm)	$V^1(\infty)$ Final Gas Volume Outside Bladder (liters)	$V^1(\infty)/V_i^1$ Final to Initial Volume Radio
Case I:			
$V_i^1 = 10$ liters	5	11.558	1.1558
	10	14.826	1.4826
	15	17.706	1.7706
	20	20.333	2.0333
Case II:			
$V_i^1 = 15$ liters	5	16.321	1.0881
	10	19.340	1.2893
	15	22.020	1.4680
	20	24.469	1.6312
Case III:			
$V_i^1 = 20$ liters	5	21.083	1.0542
	10	23.853	1.1927
	15	26.334	1.3167
	20	28.605	1.4303

As can be seen from the above table, an increase in total system pressure causes the gas space on the outside of the bladder, V^1, to increase. The gas-vapor space or bubble behind the bladder, V^2, therefore decreases under an increase in total system pressure. As can be seen, in no case did $V^1(\infty)$ reach V, the total volume occupied by gas and vapor. However, in Case III pressurization to 20 atmospheres nearly did so, although the limit of Equation (2.3.1) indicates that the vapor volume can never be totally collapsed by increasing the pressure.

2.4   Possible Mechanisms for Bubble Formation

As reported in Section 2.1, gas bubbles are observed to form and grow on the surface of the bladder which is adjacent to the liquid. A simple theory to describe the growth process was presented in Section 2.2 where it was shown that any bubble must have an initial radius greater than $2\sigma \sin \theta / p_v$ in order to grow.* While the growth of the bubble whose radii exceed a certain minimum is quite understandable on the basis of conservation of particles, the mechanism of the formation of the bubbles and their initial growth to beyond the critical size is not at all clear.

Several possible mechanisms were investigated in an attempt to explain bubble formation.

(1)   The removal of the bladder from the liquid due to increases in total pressure on the liquid side as a result of gas absorption.

(2)   The nucleation of gas bubbles on the surface of the Teflon caused by thermodynamic fluctuations in the liquid-gas solution.

(3)   The existence of microcracks in the bladder material which contain gas and from which bubbles grow due to the addition of pressurant gas by diffusion through the bladder.

Of these, the first appears extremely unlikely because no mechanism can be conceived of to generate the rather large pressures required to remove the liquid from the bladder, that is, to overcome the cohesive forces between bladder and liquid. This can be shown as follows. That part of the free energy of a liquid solid body which is due to surface tension forces is (Reference 2)

$$F_\sigma = \sigma(A - A_w \cos \theta) \qquad\qquad (2.4.1)$$

where σ is the surface tension between liquid and vapor, A is the interfacial area between liquid and vapor, A_w is the wetted area and θ is the contact angle. The free energy change in separating liquid from a solid surface can be easily obtained by taking the difference between the free energy in the states shown below.

----

*This applies to an unlaminated bladder only. For bladders constructed to have a very small leak rate even quite large bubbles would collapse due to the more rapid leakage of gas from the bubble to the liquid than its supply to the bubble through the bladder.

<div align="center">State 1   State 2</div>
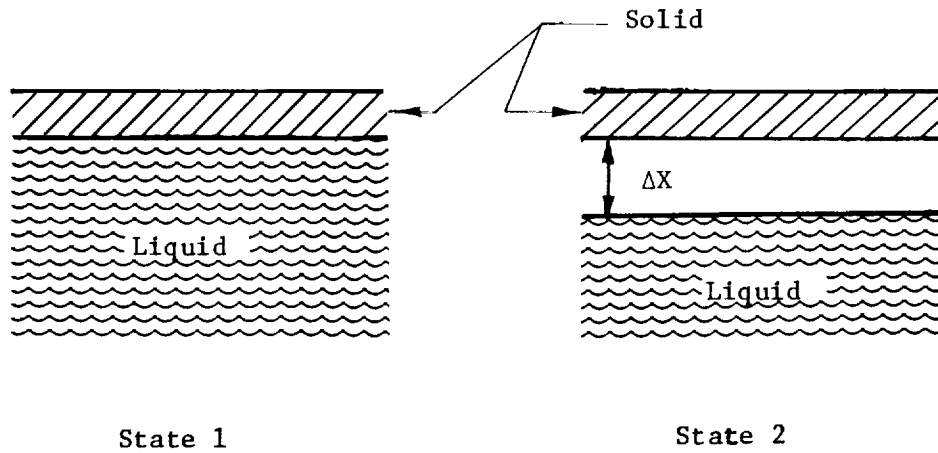
we have

$$F_{\sigma 1} = - \sigma \cos \theta \, A_w \quad \text{(since } A = 0\text{)}$$

and

$$F_{\sigma 2} = \sigma A \qquad \text{(since } A_w = 0\text{)}$$

so that

$$\Delta F_\sigma = F_{\sigma 2} - F_{\sigma 1} = (1 + \cos \theta) A \sigma \qquad (2.4.2)$$

since $A = A_w$. The work done is obtained by equating ΔF to the force times the displacement. This is

$$p_\sigma A \Delta X = \Delta F_\sigma = \sigma (1 + \cos \theta) A$$

$$p_\sigma = \frac{(1 + \cos \theta)}{\Delta X} \sigma \qquad (2.4.3)$$

That is, a pressure p_σ acting through a distance ΔX does the work ΔF. Choosing a conservative value of ΔX of about 100 molecular diameters that is, 10^{-6} cm and noting that for propellants in contact with non-wetting surfaces such as Teflon $(\cos \theta \approx 0)$ we have

$$P_\sigma \approx 10^6 \left(\frac{\text{dynes}}{\text{cm}^2} \right) \sigma \approx \sigma \, (\text{atms}) \qquad (2.4.4)$$

Thus the pressure required would be about 27.5 atms. for N_2O_4 and 78 atms. for N_2H_4. No mechanism exists capable of developing such large pressure differences.

Thermodynamic fluctuations occur even in pure homogeneous liquids causing the nucleation of vapor bubbles. In metastable states, such as a superheated liquid or a subcooled vapor, the fluctuations are responsible for setting off the processes which ultimately return the system to thermodynamic equilibrium. Thus in a sub-cooled vapor local fluctuations cause the formation of liquid nuclei which grow if they are above a certain critical size. The appearance of the liquid phase allows the system to approach thermodynamic equilibrium. We can show that the formation of gas-vapor bubbles on the surface of the bladder which are above the critical size $r_{min} = 2\sigma \sin \theta / p_v$ is extremely unlikely.

In Reference 3 it is shown that the probability of creating, due to thermodynamic fluctuations, a vapor nucleus of radius r is

$$\omega(r) = Ae^{-\frac{4}{3}\frac{\pi}{kT}\sigma r^2} \qquad (2.4.5)$$

for a spherical bubble, where A is a constant, T is the absolute temperature, and k is Boltzmann's constant. For nucleation on a surface having contact angle θ, σ must be replaced in (2.4.5) by

$$\sigma_{eff} = \left(\frac{1 - \cos \theta}{2}\right)^{2/3} \left(2 + \cos \theta\right)^{1/3} \qquad (2.4.6)$$

A calculation of the argument of the exponential in (2.4.5) will show, however, that the probability of forming any nucleus except those having molecular dimensions is extremely small. (The dominant factor is k the value of which is 1.38×10^{-16} ergs/°K). Thus the spontaneous formation of nuclei of sufficient size to grow either on the surface of the bladder or within the body of the propellant is extremely unlikely.

The result might be somewhat different if the liquid were highly supersaturated with gas since the probability of forming a given nucleus should be somewhat proportional to the degree of super saturation. However,

the mechanism by which the liquid at the bladder surface would become supersaturated is unknown.*

The presence of microcracks and surface irregularities appears to be the most promising explanation for the appearance of bubbles at this time. It is well-known that surface condition has a strong influence on the creation of nuclei at surfaces in superheated liquids (Reference 4). It could well be the dominant influence here. Gas which fills microvoids or cracks in the bladder material would grow due to the addition of gas by diffusion through the bladder faster than diffusion out into the liquid. This could occur for quite small bubble sizes or crack sizes since effectively the gas would leak into the crack over a large area on the pressurant side but could move into the liquid only at the gas-liquid interface which is quite small.

---

*The bubbles formed immediately in the tests at TRW Systems making it doubtful that the liquid was saturated with gas at the bladder surface.

3.0 MEASUREMENT OF DIFFUSION PARAMETERS

3.1 Gas-Vapor Diffusivity Measurements

In order to more realistically analyze the problem of pressurant gas disposition on the propellant side of a permeable bladder, the binary diffusion coefficients for the actual pressurant gas-propellant vapor pairs are required. These parameters were determined as a function of temperature for the following propellant vapor-pressurant gas combinations:

$$N_2H_4 - He \qquad N_2H_4 - N_2$$
$$N_2O_4 - He \qquad N_2O_4 - N_2$$
$$B_2H_6 - He \qquad B_2H_6 - N_2$$
$$OF_2 - He \qquad OF_2 - N_2$$
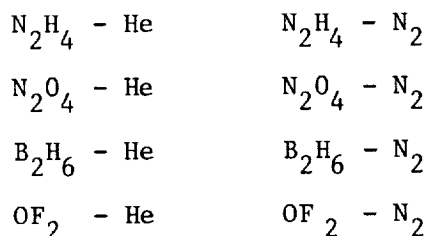
A review of the literature revealed that the current methods (References 5,6,7) other than the method used (Reference 8) to determine diffusion coefficients employ a number of time-consuming individual measurements. In the case of a point source method of Walker and Westenberg (References 7, 9,10,11), the time was somewhat shortened, but the precision of diffusion coefficient estimation was poor. In most cases, the concentration changes that are observed are measured with a thermoconductivity detector, which, if made of nickel, is compatible with the propellants to be used in this investigation. However, the apparatus used prior to the method of Giddings and Seager was not compatible with one or more of the propellants to be studied. If measurements are required at temperatures other than ambient, the use of conventional methods require elaborate thermostating chambers. For these reasons, the method of Giddings and Seager was selected.

The experimental method of Giddings and Seager used in this task involves the use of a gas chromatograph containing a long (≈ 14 m), empty 1/4 inch, i.e. diffusion tube. The diffusion coefficient was obtained by measuring the dispersion of a narrow pulse of a trace component as it is moved through the column by the carrier gas. Use was made of the equation relating height equivalent to a theoretical place in a typical gas chromatograph which can be written as:

$$H = \frac{1}{(1/2\lambda d_p) + (1/C_g V)} + \frac{2\gamma D_g}{V} + C_\ell V + C_k V \qquad (3.1.1)$$

where

λ and γ = constant of order unity

V = average carrier gas velocity

d_p = average diameter of the contained particles

D_g = binary diffusion coefficient for the sample in the carrier gas

C_g, C_ℓ and C_k = nonequilibrium terms, representing gaseous diffusion, liquid diffusion and kinetic processes, which can be calculated using the theory of gas chromatography

The plate height, H, is obtained experimentally as:

$$H = L\sigma^2 \, 1/t^2 \qquad (3.1.2)$$

where

L = column length

σ = standard deviation of the eluted peak in time units

t = retention time of the peak measured to its center

The simplest case of Equation 3.1.1 can be applied to a circular tube empty of packing and liquid absorber. It was assumed that absorption at the wall is negligible, so that $C_k = 0$. Because no liquid is contained in the tube, $C_\ell = 0$. The quantity $2\lambda d_p$ goes to infinity because there are no mixing stages in the tube. Also, for this geometry, $\gamma = 1$ (γ is called tortuosity factor). Then in this case

$$H = \frac{2D_g}{V} + \frac{r_o^2 V}{24D_g} \qquad (3.1.3)$$

where $r_o^2/24D$ replaces C_g.

An equivalent form of this expression is:

$$D_g = \frac{V}{4}\left(\sqrt{H \pm \sqrt{H^2 - r_o^2/3}}\right) \qquad (3.1.4)$$

where r_o = radius of the tube

During the present reporting period, an Aerograph 1520 gas chromato-graph was employed with a nickel thermal conductivity detector. The flow rate of carrier gas was measured with a soap film flowmeter, and the flow rate of carrier gas was controlled by means of needle valves.

The first diffusion tube used was made of standard 1/8 inch outside diameter copper tubing approximately 50 feet long. However, a 1/4 inch diameter tube was substituted because the 1/8 inch tube did not give a Gaussian peak for Nitrogen in Helium; the use of the 1/4 inch tube gave a Gaussian peak. The diffusion tube used was made by cutting a 50 foot coil of 1/4 inch diameter copper tubing into two pieces 1 and 14 meters, respectively. The lengths of both tubes and the diameter of the tubes was determined. A second set of stainless steel tubes were similarly prepared.

To correct for end effects and for diffusion occurring in the instrument dead volume, data was taken with both the long and short tubes. The data for the short tube was then subtracted from the long tube. The equation for H from which D_g was determined is:

$$H = (L_d - L_c)\,\frac{\sigma_d^2 - \sigma_c^2}{(t_d - t_c)^2} \qquad (3.1.5)$$

where subscripts d and c refer to the long and short tubes respectively.

Equation 3.1.4 used to evaluate the binary diffusion coefficient D_g yields two values of D_g for each value of H. Up to velocity $V_c = 48$ D_g/r_o the positive root of Equation 3.1.4 is taken. Beyond velocity $V = V_c$ the negative root is taken. The two values are equal when $V = V_c$. This also corresponds to the minimum value of the plate height, H. In practice it was found that for our instrument geometry, in order to obtain best precision it was necessary to use values where V_c was from 1/20 to 1/4 the value where the two roots are equal.

3-3

In order to determine if the technique was satisfactory, the diffusion coefficient for Nitrogen in Helium was determined. The values obtained agreed closely with those reported by Giddings and Seager, Reference 8, (see Table 3.1-2) hence, the technique has been adopted for this work.

Seager, et. al. (Ref. 12) have used this method for the measurement of the exponent m in the assumed T^m dependence of the gas diffusion coefficients. In this case, the oven of the gas chromatograph or a dewar containing dry ice or ice was used to control the temperature. Seager, et. al. reported that the average value for m for all gases and vapors is 1.70. Experimentally, Seager, et. al. found m to be 1.75 for the binary pair N_2 - He. Results obtained by Seager, et. al. (Reference 12) others (Reference 7, 8) and our investigation are compared in Table 3.1-2. As can be seen, there is reasonable agreement between our data and that obtained by other investigators.

Diffusion coefficients were obtained for the eight binary pairs measured, and the results are summarized in Table 3.1-3. Liquid sampling and injection of hydrazine was accomplished by a $1\mu\ell$ Hamilton syringe which was used to deliver $0.1\mu\ell$ of sample. The other propellants were expanded to 760 torr on a vacuum handling manifold. Then a Beckman gas sampling loop was used to add a 0.1 cc sample into the diffusion tubes.

Copper tubes were used in measuring the binary pairs:

$$N_2 \quad - \text{He}$$

$$OF_2 \quad - \text{He}$$

$$OF_2 \quad - N_2$$

$$B_2H_6 - N_2$$

$$B_2H_6 - \text{He}$$
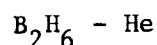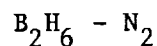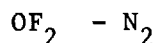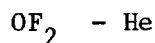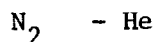
and stainless steel tubes were used with the binary pairs:

$$N_2 \quad - \text{He}$$

$$N_2H_4 - N_2$$

$$N_2H_4 - He$$

$$N_2O_4 - N_2$$

$$N_2O_4 - He$$
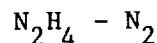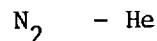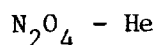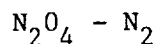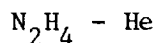
The use of the stainless steel diffusion tubes were required because both N_2O_4 and N_2H_4 react with or decompose on the surface of copper. The binary pair N_2 - He was run on both tubes to evaluate the method used.

Values for $\underline{m}$ given in Table 3.1-3 differ from the average value 1.70 by a greater amount than the values given by Seager, et. al. (Reference 12). This could be the result of experimental errors and the fact that measurements were made at two or three temperatures instead of a large number of temperatures thus giving a less accurate estimate of $\underline{m}$. A limited number of temperatures were used because of the difficulty in handling some of the propellants. Seager, et. al. limited their study to benzene and normal alcohols which are much easier to handle than the present propellants. When propellants are investigated, not only would the experimental errors be expected to be greater; but attractions between molecules and between the propellant and the diffusion tubes could alter the value for the exponent $\underline{m}$.

A more likely explanation for the variations in $\underline{m}$ is that the propellants either contained a small amount of impurities or the propellant decomposed either in the diffusion tubes or in the sample handling equipment. Both N_2O_4 and OF_2 react with metal surfaces. Vapors of N_2H_4 tend to decompose when in contact with metal surfaces to form N_2, H_2, and NH_3. If B_2H_6 is exposed to temperatures above $0°C$, some decomposition takes place according to the following reaction:

$$B_2H_6 \rightarrow B_4H_{10} + B_5H_9 + B_{10}H_{14} + (BH)_x + H_2 \qquad (3.1.6)$$
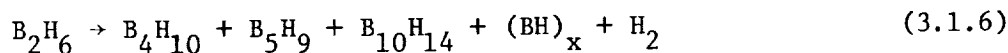
Before each diffusion measurement was made for B_2H_6, the B_2H_6 was condensed, and the hydrogen removed by pumping on the sample with a vacuum pump. The other impurities could not be easily removed.

Three component systems were treated by Fairbanks and Wilke (Reference 13) and experimentally evaluated by Giddings and Seager

3-5

(Reference 8). The equation for the diffusion coefficient of a trace
sample of one gas into a mixture made up of two gases is:

$$D_{mix-1} = \left[\frac{X_2}{D_{2-1}} + \frac{X_3}{D_{3-1}} \right]^{-1}$$ (3.1.7)

where X_2 and X_3 are the mole fractions of the two gases making up the
mixture and D_{2-1} and D_{3-1} are the diffusion coefficients of the gases
making up the mixture in the sample gas.

From the consideration of Equation (3.1.7), one can see that small
amounts of an impurity with a diffusion coefficient that differs greatly
from the diffusion coefficient of the major component will result in a
large error in the measured diffusion coefficient.

The theoretical estimates of the binary diffusion coefficients
presented in Appendix 7.3 requires knowledge of at least one transport
property, say, thermal conductivity, for each component. However, the
thermal conductivities were not known for vapors of the propellant studied.
A rough estimate of the thermal conductivities can be obtained with the
thermoconductivity cell of the gas chromatograph according to the relation.

$$\frac{T_1}{T_2} = \frac{A_1/V_1}{A_2/V_2}$$ (3.1.8)

where

T_1 = the thermal conductivity of a reference substance, such as N_2,
at a given pressure temperature

T_2 = thermal conductivity of substance to be determined

A_1 = peak area of reference

A_2 = peak area of substance to be determined

V_1 = volume of reference

V_2 = volume of substance

3-6

By comparing the area as measured on the gas chromatograph of an equivalent amount of N_2 or ethanol with the area measured for vapors of the propellants the approximate thermoconductivities given in Table 3.1-1 were obtained. All instrumental conditions were maintained constant for the reference gas used and the propellant measured.

TABLE 3.1-1

APPROXIMATE THERMAL CONDUCTIVITIES

Propellant	Temperature °C	Thermal Conductivity cal/(sec)(cm^2)(°C/cm) x 10^{-6}
Hydrazine	77	62.5
Nitrogen Tetroxide	88	47.7
Diborane	26.7	54.0
Oxygen Difluoride	26.7	66.8

TABLE 3.1-2

DIFFUSION COEFFICIENTS OF BINARY SYSTEM
CORRECTED TO 760 TORR

Temp °C	$D(cm^2/sec)$ $He-N_2$
25	0.692
	let. values
	0.688 (4)
	0.687 (3)
	Seager et. al. values (8)
25	0.687
50	0.766
80	0.893
110	1.077
140	1.200
	Stainless Tube Results
50	0.790
105	0.953
135	1.063
	Copper Tube Results
20	0.669
40	0.721

TABLE 3.1-3

EXPERIMENTAL DIFFUSION COEFFICIENTS

Temp. °C	N_2H_4-He	N_2H_4-N_2	N_2O_4-He	N_2O_4-N_2	OF_2-He	OF_2-N_2	B_2H_6-N_2	B_2H_6-He
-77							0.146	.349
0					0.500	0.100	0.235	.423
20								
24			0.736		0.611	0.122		
40								
46					0.636	0.225		
60		0.481						
61	0.592			0.405				
89								
92			0.838					
94	0.678							
147			0.918					
149		0.900						
153	0.814							
$\underline{m}$	0.875	2.65	1.65	1.32	1.69	3.32	1.33	2.09

3.2   Gas-Liquid Solubility and Diffusivity Measurements

The purpose of the experimental measurement of pressure and gas diffusion and solubility in liquid earth storable propellants is to provide the necessary data to support the analysis of bladder permeation and bubble growth. The practical importance of these data has been emphasized recently with the correlation of engine performance deterioration with propellant degassing during flow (cf. Reference 15). Consequently, knowledge of diffusion rates and solubility as a function of time, temperature and pressure is of practical necessity in the establishment of engine operating conditions, i.e., pressurization-expulsion-venting cycles.

In this portion of the study, the rates of diffusion and solubility of two gases, helium and nitrogen, have been determined in hydrazine and in nitrogen tetroxide. For the nitrogen/N_2O_4 pair, measurements were made between 24°C (57.2°F) and 60°C (140°F), for helium/N_2O_4, 0°C (32°F) and 40°C (104°F), for nitrogen/N_2H_4, 24°C (75.2°F) and 60°C (140°F), and finally, for helium/N_2H_4, 24°C (75.2°F) and 60°C (140°F). The initial pressurization level was maintained at a constant level (approximately 250 psia (17 atm)) to eliminate consideration of that variable.

The nitrogen tetroxide used in this portion of the study conformed to NASA specification MSC-PPD-2A, while the hydrazine utilized conformed to military specification MIL-P-26536B.

The apparatus used for the experimental measurement of diffusivity and saturation is presented schematically in Figure 3.2-1. The apparatus consists of a 335 ml stainless steel cylinder (A) with stainless steel lines making the appropriate connection to the pressurant supply tank and safety vent. The cylinder is equipped with a 0-300 psia Tabor pressure transducer (T) with an accuracy of ± 0.25% of full scale. Transducer power was supplied by 10 volt power supply and pressure readout was accomplished using a shunt caliabration system (D) and a Non-Linear Systems, Inc. X-2 Digital Multi-meter (F). The multimeter has a range of .01 mv to 119.99 mv, a response time of 500 milliseconds and an accuracy of 0.05% of reading plus 0.5% of full scale. Temperature control was accomplished using a water bath (B) equipped with a Bronwill Thermal Controller which allowed temperature control of ± 0.1°C to be maintained.
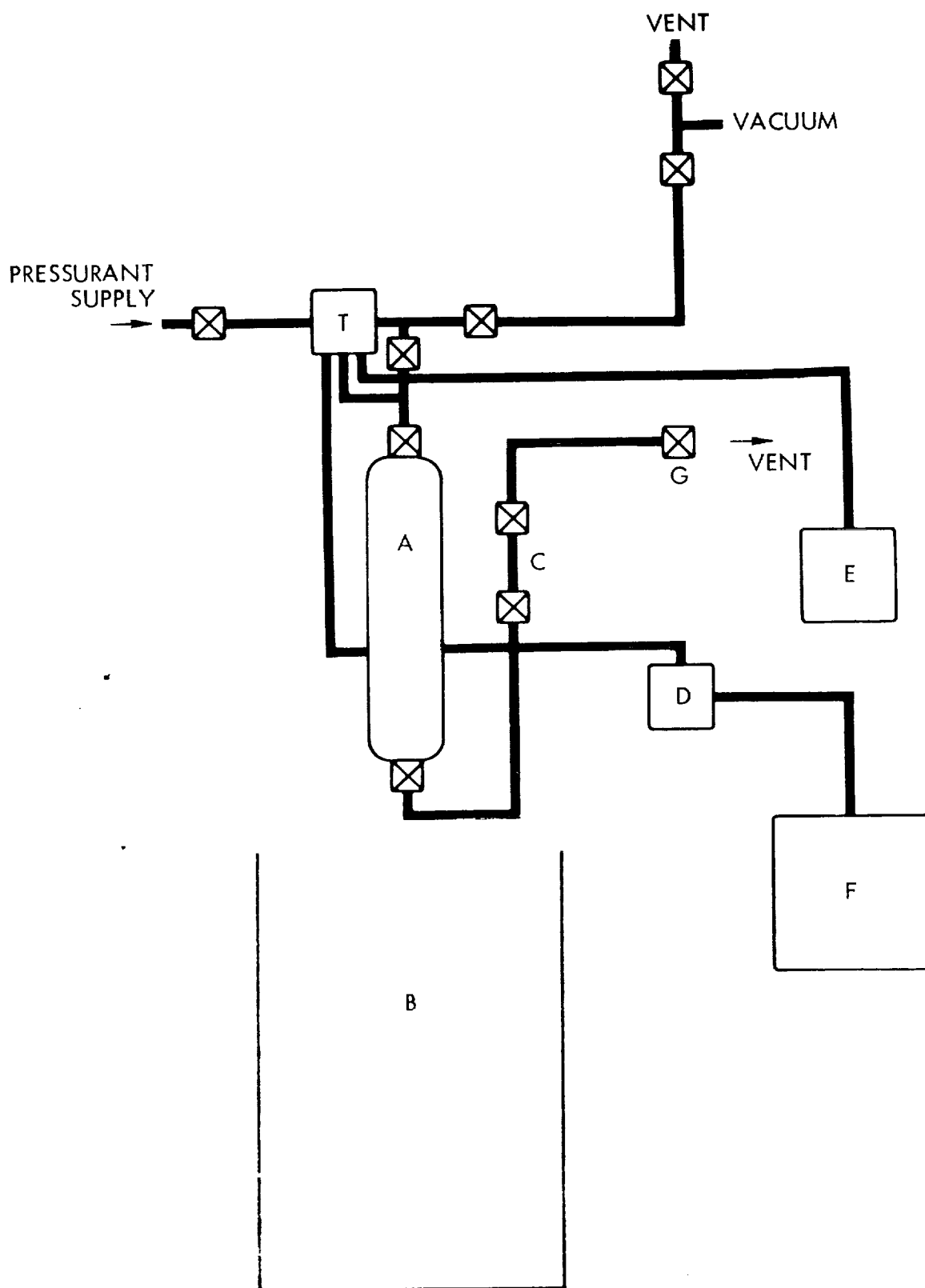
Figure 3.2-1. Diffusivity Measurement Apparatus

The principle of operation of the apparatus is based on the fact that the rate of pressure decay of a gas over a liquid is diffusion limited, i.e. rate of pressure decay can be equated to diffusion rate, provided external mixing phenomena such as thermal gradients and vibration, are obviated. Then, by utilizing a known ullage and weight of propellant, the quantity of gas dissolved per unit weight of propellant (saturation level) can be computed from the appropriate mathematical relationships described in detail below.

The experimental parameters required for computation of diffusivity and saturation level were measured for all propellant/pressurant gas combinations in the following way. A known quantity of propellant was introduced into the volume calibrated saturation cylinder (A), using vacuum techniques. The cylinder was placed in the bath and allowed to equilibrate thermally. When at thermal equilibrium, pressurant gas at the temperature of the bath was introduced rapidly into the ullage volume of the cylinder until the desired total gas pressure was obtained as indicated by the pressure transducer (P). The regulated source of pressurant gas was then isolated from the diffusion apparatus and measurements of pressure decay were initiated. Pressure decay measurements were recorded frequently during the rapid transient period, and then infrequently during the remainder of the diffusion process where the observed ΔP's were rather small. When the quiescent system displayed no apparent pressure drop (8 to 36 hours), the cylinder was agitated vigorously to insure complete saturation equilibrium and the final pressure was recorded.

The diffusion of a gas into a liquid is described mathematically by a relationship originally derived to describe diffusion into a plane (Reference 16). The ratio of the mass absorbed by the bulk liquid at any time t, M_t, to the total mass absorbed at infinite time, M_∞, is defined by the equation

$$\frac{M_t}{M_\infty} = 1 - \sum_{n=1}^{\infty} \frac{2\alpha(\alpha + 1)}{1 + \alpha + \alpha^2 q_n^2} \, e^{-Dq_n^2 t/\ell^2} \qquad (3.2.1)$$

where

α is the fractional uptake of the gas by the bulk liquid

$$\frac{1}{1 + \alpha} = \frac{M_\infty}{M_o} \qquad (3.2.2)$$

M_o is the mass of the solute originally in the gas phase

D is the diffusion coefficient

ℓ is the depth of the liquid

t is elapsed time, and

q_n is the nth successive root of the equation

$$\tan q_n = -\alpha q_n \qquad (3.2.3)$$

The measured experimental variables are weight of solvent, w, ullage volume, V_u, liquid depth, ℓ, and pressure, p, as a function of time, t. The pressures are first corrected to determine the partial pressure of the solute gas by subtracting the measured vapor pressure of the pure solvent. These partial pressures are related to partial gas density using the perfect gas law

$$\rho = \frac{PM}{RT} \qquad (3.2.4)$$

where M is the molecular weight of the solute gas. Letting

ρ_o = density of the solute gas at time zero (before diffusion has occurred)

ρ_t = gas density at time, t

ρ_∞ = gas density at infinite time

the key parameters of Equation (3.2.1) may be defined as follows

$$\frac{M_t}{M_\infty} = \frac{\rho_0 - \rho_t}{\rho_0 - \rho_\infty} \tag{3.2.5}$$

$$\alpha = \frac{\rho_\infty}{\rho_0 - \rho_\infty} \tag{3.2.6}$$

Using Equation (3.2.5) Equation (3.2.1) may be written as follows

$$\rho_t = \rho_0 - (\rho_0 - \rho_\infty) \left[1 - \sum_{n=1}^{\infty} \frac{2\alpha(\alpha + 1)}{1 + \alpha + \alpha^2 q_n^2} e^{-Dq_n^2 t/\ell^2} \right] \tag{3.2.7}$$

which describes density directly as a function of time with three parameters, ρ_0, ρ_∞, and D. The density at infinite time, ρ_∞, was determined following the measurement of density as a function of time by vigorously shaking the liquid with the gas and allowing the system to reequilibrate. The pressure was measured and this final density determined. Although it appears possible to measure ρ_0 directly, it cannot be accomplished since a finite time is required to charge the pressure vessel and for liquid-vapor equilibrium to become reestablished after charging. It is therefore necessary to determine both ρ_0 and D from the ρ_t data.

The technique utilized to determine the remaining parameters is based on the truncated Taylor expansion of Equation (3.2.7) in terms of ρ_0 and D.

$$\rho_t = \rho_t^o + \left(\frac{\partial \rho_t}{\partial \rho_o}\right)^o \Delta \rho_o + \left(\frac{\partial \rho_t}{\partial D}\right)^o \Delta D \tag{3.2.8}$$

where D^o is an estimate of D

ρ_t^o is an estimate of ρ_o

ρ_t^o, $\frac{\partial \rho_t}{\partial \rho_o}$, and $\frac{\partial \rho_t}{\partial D}$ are evaluated at D^o, ρ_o^o

$$\Delta D = D - D^o$$

$$\Delta \rho_o = \rho_o - \rho_o^o$$

Four separate binary gas-liquid diffusion systems were examined in the experimental program: N_2/N_2O_4, N_2/N_2H_4, He/N_2O_4, He/N_2H_4. The diffusion experiments were performed at three different temperatures in order to indicate the dependence of the diffusivity upon temperature. The pressure was held over a narrow range to eliminate the consideration of that variable.

The experimental data were reduced using a time-sharing computer program based on the mathematical model described in the previous section. The program is designed to accept raw pressure (m.v.) data and convert it into the necessary partial density.

Since Equation (3.2.8) is linear in ΔD and ρ_o, regression analysis may be applied to determine new estimates for D and ρ_o from the observed ρ_t data, $D^o_{new} = D^o_{old} + \Delta D$, $\rho_{o\ new} = \rho_{o\ old} + \Delta \rho_o$. Using these new estimates the function and its derivatives can be reevaluated and regression applied again. This procedure is continued until successive values of D^o and ρ_o^o are within some prescribed tolerance. The diffusivity is then directly defined and solubility, S, may be determined from the expression

$$S = 22400 \times V_u \times (\rho_o - \rho_\infty)/(M \times W) \quad (cc(STP)/g) \qquad (3.2.9)$$

The diffusivity results and their error estimates $\sqrt{S_D^2}$ for the various systems are summarized in Table 3.2-1 for the various temperatures. Also tabulated are the solubilities and final gas partial pressures.

The coefficients A and B of an Arrenhius type function describing the behavior of diffusivity as a function of temperature

$$D = Ae^{-B/T}$$

were determined from the reduced data. The estimates for A and B are summarized in Table 3.2-2.

Table 3.2-1

DIFFUSIVITY AND SOLUBILITY DATA

Temp (°C)	$D(cm^2/sec)$ $\times 10^5$	$\sqrt{S_D^2}$ $\times 10^5$	S(std cc/g)	$K\left(\dfrac{std\ cc}{cm^3\ atm}\right)$ $\times 10^3$	P_F (atm)
			N_2/N_2O_4		
24.	7.4	0.3	1.67	212.	11.49
40.	7.8	0.2	1.63	220.	10.71
60.	14.7	0.1	1.50	260.	8.23
			He/N_2O_4		
0.	21.9	3.4	0.250	23.	15.85
24.	55.0	10.6	0.297	29.	14.71
24.	46.6	2.3	0.330	36.	13.37
40.	24.4	1.7	0.352	39.	13.01
			N_2/N_2H_4		
24.	16.1	4.0	0.042	3.95	15.64
40.	24.5	4.1	0.051	4.80	15.45
60	52.5	4.4	0.075	7.22	15.09
			He/N_2H_4		
24.	74.1	55.3	0.021	1.90	16.02
24.	77.7	18.2	0.024	2.10	16.58
40.	31.0	15.1	0.032	2.81	16.53
60.	58.9	26.5	0.039	3.43	16.50

Table 3.2.2

COEFFICIENTS FOR $D = Ae^{-B/T}$

SYSTEM	$A(cm^2/sec)$	$B(°K)$
N_2/N_2O_4	4.05×10^{-2}	1900.8
He/N_2O_4	3.13×10^{-3}	651.9
N_2/N_2H_4	8.28	3235.9
He/N_2H_4	2.206×10^{-5}	-1005.8

3.3 Experiments With Laminated Sample

The bubble growth experiments performed with the specially prepared FEP-Aℓ-FEP laminate were described in Section 2.1. No gas bubbles were observed on the liquid side of the bladder sample even over a period of 5 days. Permeation experiments were attempted with the sample after these bubble growth tests. The bubble growth test cell was loaded with unsaturated hydrazine on one side of the sample and He on the opposite side and pressurized to 2 atm. The pressure decay was then monitored as a function of time using a mercury nanometer. However, the total pressure decay observed on the He side was too great to be attributed solely to the diffusive uptake of He by the liquid hydrazine and was probably due to leakage out of the test cell through the badly delaminated bladder sample.

4.0   EXTENSION OF THE PHASE I ANALYSIS

4.1   Leakage Through Laminated Bladder Structures

During Phase I of this program the permeation of the pressurant gases N_2 and He and propellant vapors N_2O_4 through laminated bladder samples was studied both experimentally and analytically. These studies ignored the presence of the liquid propellant which is, for some parts of a spacecraft mission, quite a resonable assumption. For example, during ground hold and launch the existence of strong temperature gradients and large acceleration levels insures the presence of large free convection currents and, perhaps, sloshing motions in the liquid propellant. These effects serve to mix the pressurant gas in the liquid propellant at a rate much greater than would be the case if molecular diffusion were the only mechanism for pressurant gas to enter the liquid. In the cases where this strong mixing is present in the liquid the main resistance to the transfer of mass of pressurant gas out of the ullage space surrounding the bladder is through the bladder itself, and the liquid can be ignored. However, for some phase of a spacecraft mission, say, a long low or zero-g coast, thermal convection currents and sloshing amplitudes are very weak. In these cases the liquid propellant presents a significant resistance to the transfer of pressurant gas from the gas space outside the bladder into the liquid propellant. It is for these mission periods that the work of this second phase was undertaken.

In order to determine the rate of diffusion of pressurant gas through a laminated bladder structure into a body of quiescent liquid propellant we study the following configuration (see Appendix 7.1 for a complete derivation). Consider a system consisting of a laminated bladder with a circular hole in the diffusion barrier and with pressurant gas at pressure p_o on one side and liquid propellant on the other. Since the diffusion coefficient is of the same order of magnitude in the bladder and the liquid while the thickness of the bladder is typically three or more orders of magnitude less than a characteristic dimension in the liquid, we may ignore the concentration transients in the bladder. The steady state leakage rate across a laminated bladder was found to depend on the concentration difference ΔC. We now account for the presence of the liquid

by solving the diffusion equation in the liquid propellant using as a boundary condition the steady-state leakage rate found during Phase I but where now the concentration difference across the bladder, ΔC, can change with time as the concentration in the liquid at the liquid propellant-bladder interface changes. This problem is solved in Appendix 7.1 for the total amount of pressurant gas leakage up to time T.

$$\frac{J(T)}{C_o} = \frac{f}{\varepsilon} e^{\varepsilon T} \left(1 - \Phi\left(\sqrt{\varepsilon T}\right) \right) + \frac{4f}{\varepsilon\sqrt{\pi}} \left(\sqrt{\varepsilon T} - \frac{\sqrt{\pi}}{4} \right) \tag{4.1.1}$$

where

$J(T)$ = Total leakage, gms

C_o = concentration in bladder on pressurant side

Φ = error function

where $\varepsilon = \dfrac{K_2^2 f^2}{K_\ell^2 \rho_\ell^2 D_\ell A_e^2}$

and K_2 = solubility of pressurant gas in the bladder adjacent to liquid

K_ℓ = solubility of pressurant gas in the liquid propellant

D_ℓ = diffusivity of pressurant gas in the liquid propellant

ρ_ℓ = density of the liquid propellant

A_e = effective bladder area for leakage (radius equal to 10 hole radii)

f = known function of the permeabilities of the teflon layers, their thicknesses and the hole radius in the metallic diffusion barrier (Reference 1, p. 2-8)

This expression can be used to obtain the fraction of saturation present in the liquid propellant at any time during a mission for various values of hole radius and Teflon thicknesses. Figure 4.1-1 is a plot of the dimensionless leakage rate, $j(t)/fc_o$ as a function of the nondimensional time t. Figure 4.1-2 gives the total integrated leakage rate in dimensionless form $J(T)/fc_o$ as a function of the dimensionless time T. By means of these two curves one can calculate both the instantaneous leakage rate and the accumulated leakage rate through laminated bladders containing circular holes in the diffusion barrier.
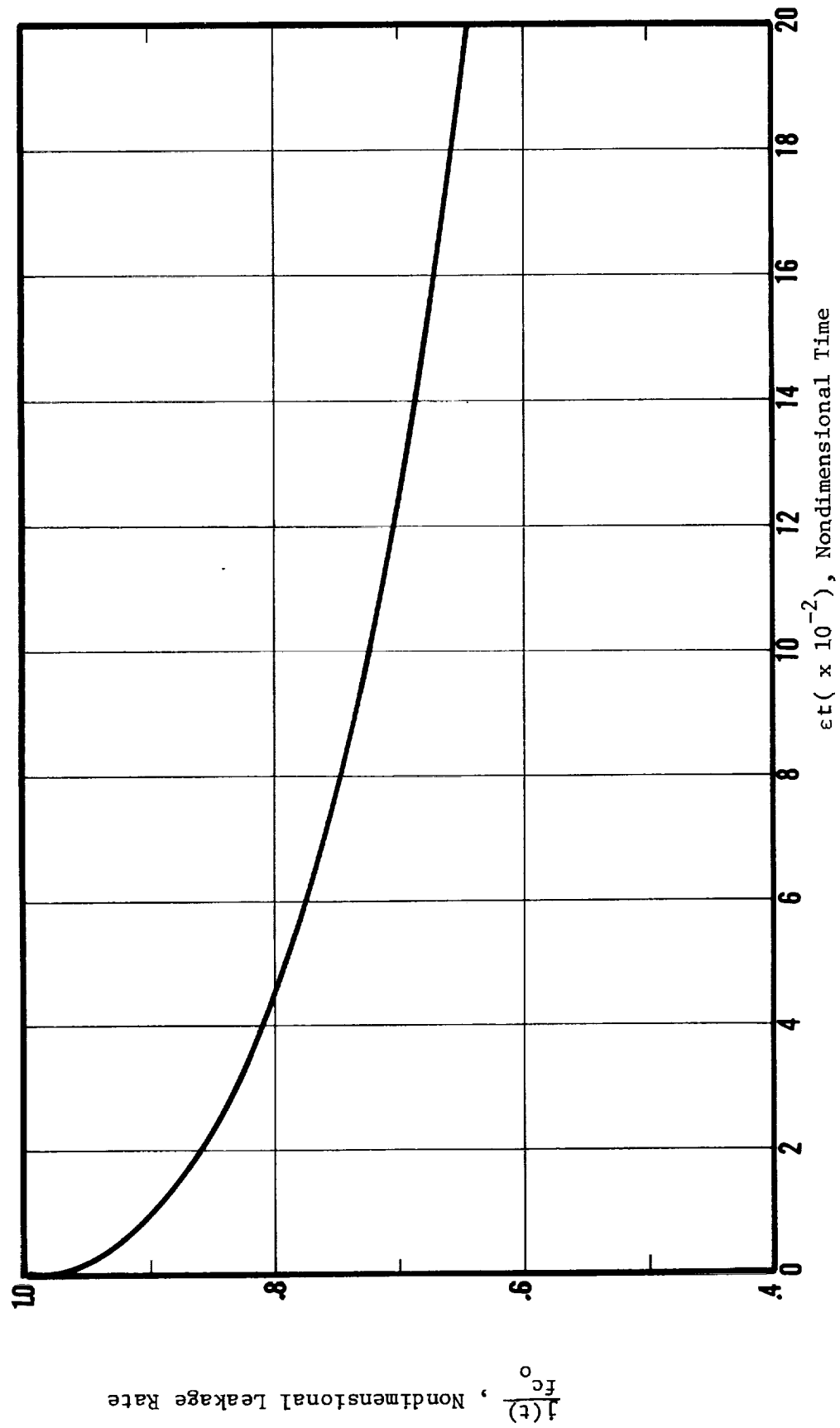
Figure 4.1-1 Leakage Rate Through Laminated Bladder with Circular Hole in the Diffusion Barrier

x-axis: $\epsilon t (\times 10^{-2})$, Nondimensional Time

y-axis: $\dfrac{j(t)}{j c_0}$, Nondimensional Leakage Rate
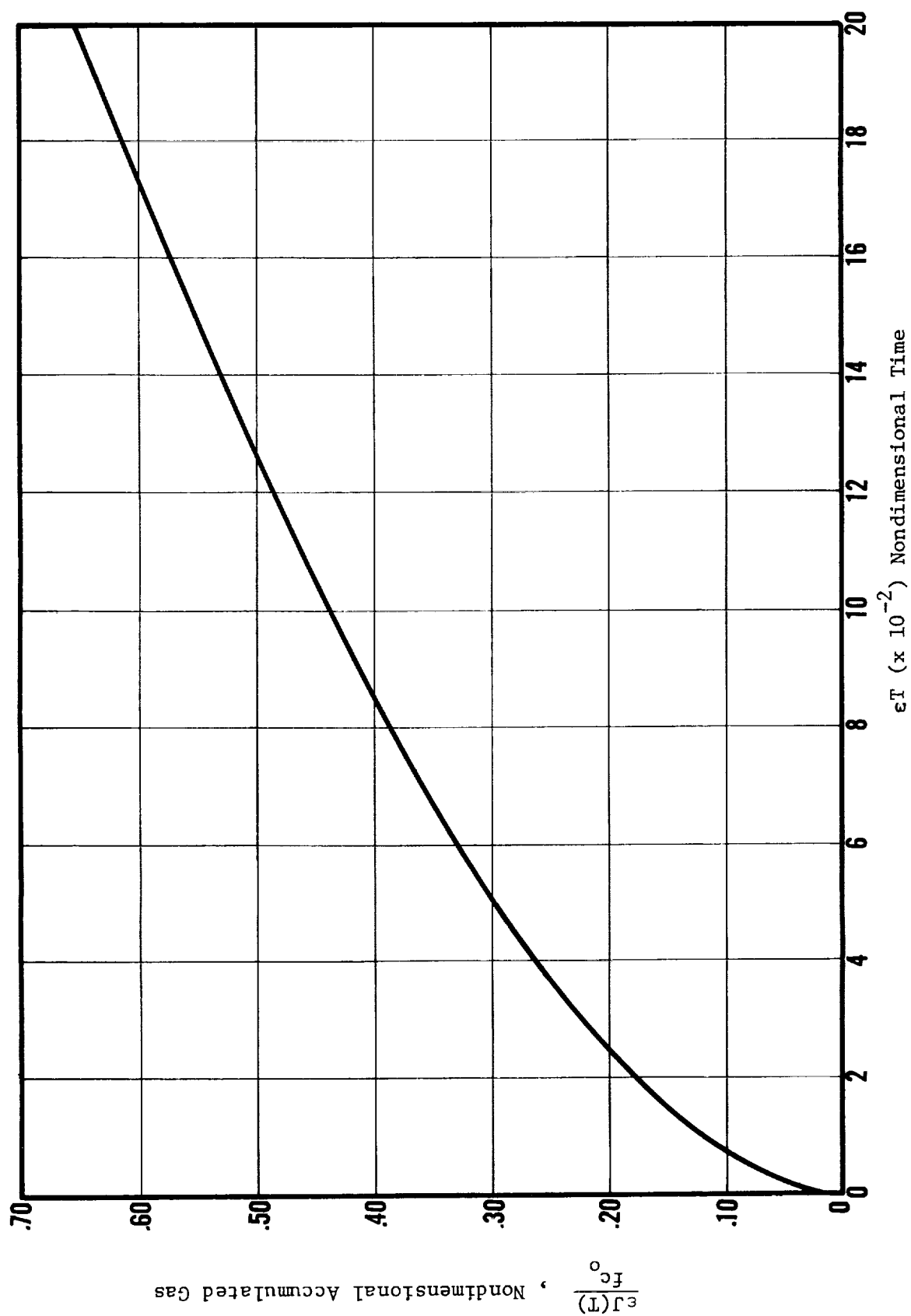
Figure 4.1-2 Integrated Leakage Through Laminated Bladder with Circular Hole in the Diffusion Barrier

4.2   Modification of Phase I Computer Program

The Diffusion Analyzer Program (DAP) developed and delivered to
JPL under Phase I of this contract dealt with the leakage of pressurant
gas through a laminated bladder with holes in the metallic diffusion barrier.
During the present study this code has been modified to include the growth
of pressurant gas bubbles assumed to be spherical segments with the appropriate
contact angle (c.f. Figure 2.2-1) on the bladder surface due to the addition
of pressurant gas by way of diffusion across the bladder and the loss of
pressurant gas from the bubble by diffusion into the liquid. The modified
DAP code will allow the calculation of bubble growth rate of an arbitrary
number of gas bubbles with any initial radius and located at any initial
position on the surface of the bladder with respect to the hole in the
metallic diffusion barrier. In addition, the capability of monitoring the
growth of a new bubble, formed when two or more bubbles combine, is
included. Normal output is composed of the bubble number, its radius and
the particular value of time (specified by the user). When two or more
bubbles are touching or their boundaries overlap, this information is
printed out as a "coalesce event" giving the numbers of the bubbles which
have combined, the surface radius of the new bubble form by them and its
new position on the bladder surface. In addition, at each point in time a
force balance between bouyancy (if a gravity field is present) and surface
tension made to determine when a bubble breaks away from the bladder surface.
When this does occur, it is so noted in the output with the bubble number
and time of breakaway. An exact description of the input functions is
included in the Design Guide.

A sample bubble growth problem was run using the modified DAP
program for a 5 mil thick slab of TFE Teflon bounded on one side by an
impermeable barrier and with a 20 mil diameter hole and on the other side
by liquid propellant. The problem was run for 5.1 minutes of machine time,
which corresponded to 1.07 hours in real, or problem, time. The initial
bubble locations assumed for this case are shown in Figure 4.2-1. During
the course of the run, normal printout occurred giving the bubble radius
as a function of time and indicating that, at 2.3 seconds after the
beginning of the problem, bubbles 1 and 3 had coalesced and that at 505.4
seconds later this new bubbles combined with bubble number 4. A contact
angle of 90° was assumed.
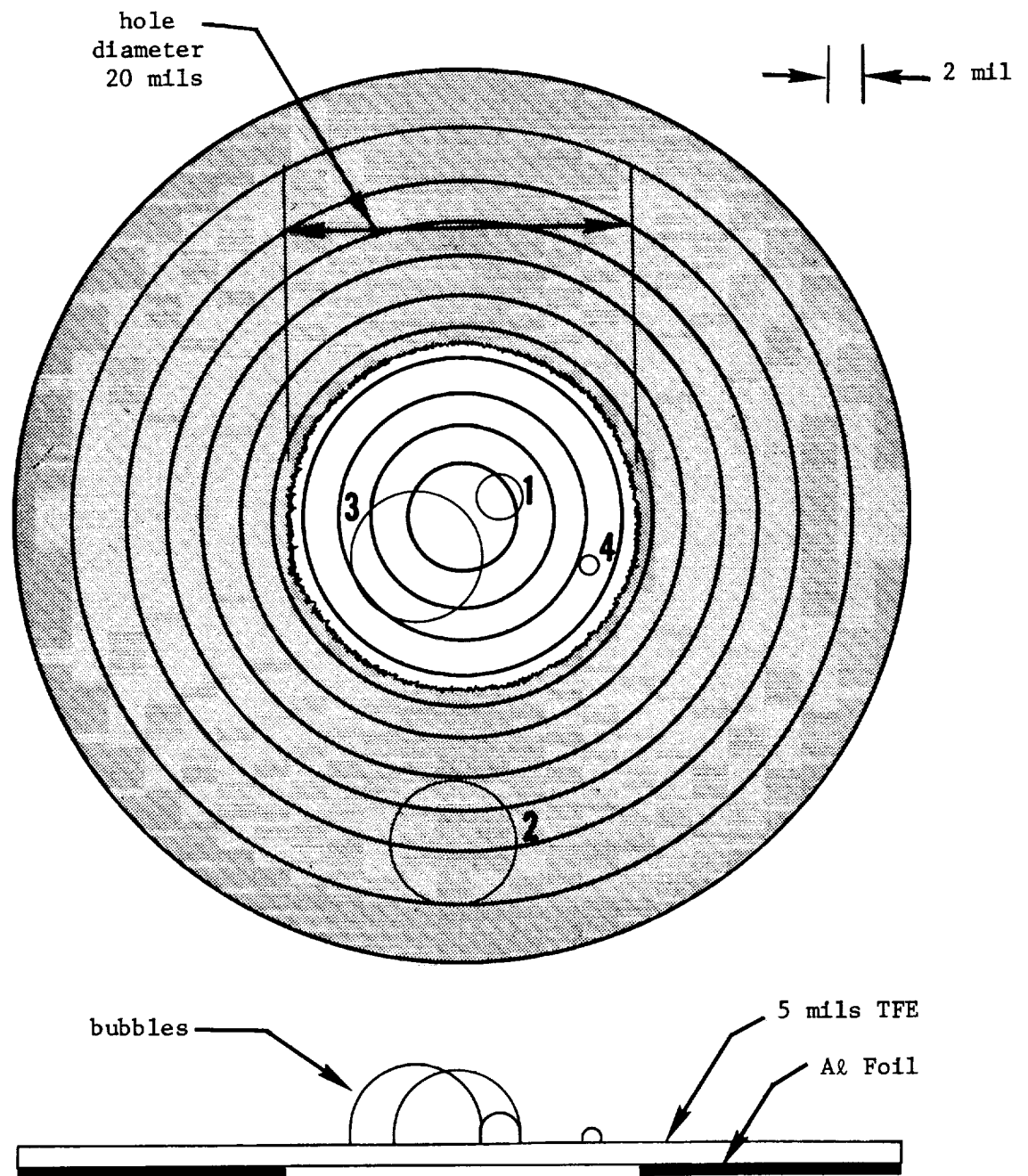
Figure 4.2-1 DAP Test Case Initial Bubble Configuration

5.0   APPLICATION AND FURTHER RESULTS
5.1   Effect of Body of Gas on Further Permeation

It was shown in Appendix A of Reference 1 that the diffusion in the gas space adjacent to a laminated bladder structure could be ignored in calculating the leakage through a laminated structure containing holes in the barrier and that to a very good approximation the surface of the bladder could be assumed to be exposed to a constant gas pressure. It seems reasonable to suppose that the same circumstances prevail when there is a gas-vapor mixture present on the liquid side of the bladder. The reason is, of course, that gas transport through gas or gas-vapor mixtures is much more rapid than that through Teflon, Teflon laminates or liquid propellants so that effectively the gas phase offers little resistance to gas transport compared to the other materials present. This was verified during the present phase of this study when the diffusion coefficients for pressurant gases in propellant vapors and in liquid propellants were determined experimentally. Referring to Sections 3.1 and 3.3 it is seen that the diffusion coefficient of pressurant gases in propellant vapors is of the order of 10^{-1} cm^2/sec while that for pressurant gases in liquid propellants is of the order of 10^{-4} cm^2/sec. The time, T, for pressurant gas to traverse a characteristic dimension, L, is given by

$$T_\ell = \frac{L_\ell^2}{D_\ell}$$

for the liquid propellant and by

$$T_v = \frac{L_v^2}{D_v}$$

for a propellant vapor space, or bubble. Even if the characteristic lengths are of the same order for both liquid propellant and propellant vapor, a highly undesirable situation as far as engine operation is concerned, the ratio of characteristic diffusive transient time in the liquid to that in a vapor space is still of the order of 10^{-3}. Therefore, the resistance offered by a vapor space to the diffusive flow of pressurant gas is negligible when compared with that offered by the liquid propellant.

5.2   Most Probable Position of Gas in a Zero-G Environment

To determine the most probable position of a gas bubble on the liquid side of the bladder in a long term zero-g environment, the difference in free energy between possible configurations is determined. It is of interest to investigate the location of gas bubbles inside a bladder since their growth rate depends upon their location, i.e., whether they are in contact with the bladder or not. In addition, wall bound bubbles would not be swept into the tank drain after engine restart as easily as would bubbles floating free in the main body of the propellant.

The most probable position for these gas bubbles will be where the free energy is a minimum. Consider the possible configurations shown schematically in Figure 5.2-1. The Helmholtz free energy for a spherical bubble or a segment of a spherical bubble is given by

$$F = \sigma A_c + F_o$$

where $F_o = U_o + TS_o$, U_o being the internal energy of the liquid phase and S_o being the entropy of the liquid phase. A_c is termed the capillary area and is defined as

$$A_c = A_1 + \cos \theta \, A_{nw}$$

where A_1 is the liquid vapor interface area, θ is the solid-liquid contact angle, A_{nw} is the non-wetted bladder contact area and σ is the liquid surface tension.

For a bubble floating free in the liquid (configuration A of Figure 5.2-1) A_{nw} is zero and $A_1 = A_1 = 4\pi r^2$. For a wall bound bubble formed by a spherical segment with contact angle, θ, (configuration B of Figure 5.2-1).

$$A_1 = A_2 = 2\pi r^2 (1 + \cos \theta)$$

$$A_{nw} = A_3 = \pi r^2 \sin^2 \theta$$

The difference in free energy between a free bubble and a wall bound bubble in an isothermal system is then

$$F_{a-b} = \pi r^2 \sigma (2 - 3 \cos \theta + \cos^3 \theta)$$

which is positive for all values of r and θ. The most probable location for gas bubbles formed inside the bladder is therefore on the inside bladder surface since the free energy is minimum there.
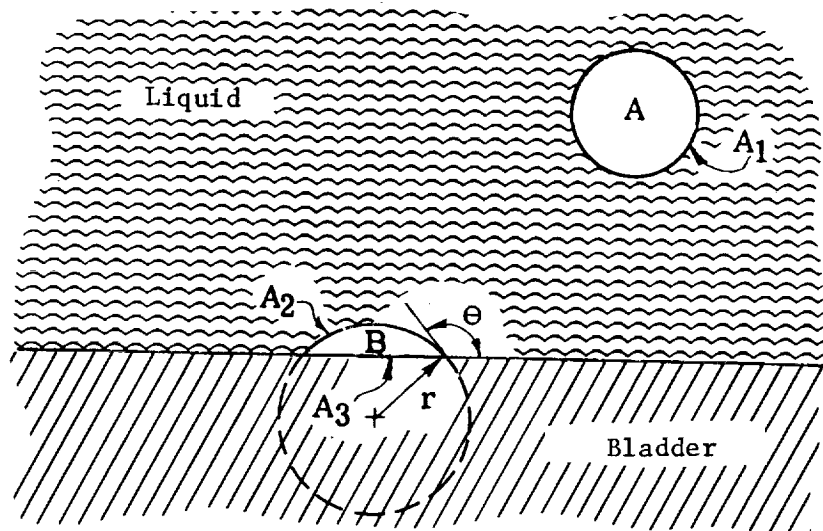
Figure 5.2-1 Possible Bubble Configurations

5.3   Applicability of Vapor Permeation Measurements to Liquid Permeation

Knowledge of the disposition of pressurant gas on the liquid side
of the bladder, i.e. whether it exists as a distinct bubble or is dissolved
uniformly in solution, depends on the rate of permeation of propellant
molecules through the bladder by diffusion. The permeation measurements
performed and reported during Phase I of this study were for propellant
vapor in contact with the bladder materials TFE and FEP Teflon. Since the
chemical potentials are identical for a liquid and for its vapor when they
are in contact at thermodynamic equilibrium, the concentration of penetrant
propellant molecules in the surface layer of the bladder should be identical
regardless of whether liquid or vapor is in contact with the bladder. The
permeation rate, assuming pure molecular diffusion, should therefore be the
same for both cases.

Stannett and Vasuda in a paper entitled "Liquid Versus Vapor
Permeation Through Polymer Films," (Ref.17) have performed experiments to
study this question for methyl alcohol and water permeating through films
of polyethylene and Mylar. Their results agree with those of Reference 18
and indicate that the permeation is independent of vapor partial pressure
and is within 16% of the value when liquid was placed in contact with the
membranes. Their results for the permeation rate of water molecules through
Mylar 100A are given in Table 5.3-1 below. Also given are the constants for
an Arrenhius type relationship, $P = P_o \exp (-E_p/RT)$, describing the temperature
dependence of permeability.

Table 5.3-1.   Permeability of Water Through Mylar 100A

	Vapor Contact 10% to 90% Relative Humidity	Liquid Contact
P cc(STP) mm/cm^2/sec/cm Hg)@ 20°C	1.49×10^{-7}	1.72×10^{-7}
E_p (kcal/mole)	0.5	1.1
P_o(cc(STP) mm/cm^2/sec/cm Hg)	3.44×10^{-7}	10.9×10^{-7}

A similar behavior was observed with water in a number of other polymers (Reference 19). In the experiments reported by Sivadjian and Riberio (Reference 20) the permeability of FEP Teflon to water and water vapor was measured by a hydrophotographic technique in which specially prepared photographic plates were sealed inside an evacuated bag made of a thin (45μ) film of FEP Teflon. The permeability of the Teflon was determined by placing it in contact with the test environment, either water vapor or liquid water. The density of the developed plates was related to the amount of moisture which had permeated through the initially evacuated bag. Permeability results obtained in this way are entered in Table 5.3-2 below.

TABLE 5.3-2

PERMEABILITY OF FEP TEFLON TO LIQUID WATER AND WATER VAPOR
IN UNITS OF cc(STP) mm/cm^2/sec/cm Hg x 10^{-5}

Permeating Medium	25°C	35°C	45°C	55°C	65°C	75°C	85°C	95°C
Water	0.048	2.64	6.6	7.55	11.8	29.00	89.8	156.0
Water Vapor	0.025	0.77	5.25	7.20	10.8	27.40	86.0	154.0

It is seen that the difference between permeability to liquid water and to water vapor is greatest at the lower temperatures and decreases to about 1.2% at a temperature of 85°C.

No data was found in the literature which dealt with the difference in the permeability of TEP or FEP Teflon to the propellant liquids or vapors of interest in this study.

If the propellants N_2H_4 and N_2O_4 behave in the same manner as water as regards permeation through Teflon, the bubble growth experiments reported during this study indicate the effect of the greater permeability of the Teflon bladders to liquid propellant when compared to that measured with vapors would be to decrease the bubble growth rate from its expected value when the permeability measured for vapor is used. This can be seen from Equation 2.2.3, which gives as expression for the driving

force for pressurant gas permeation into a bubble, and from Equation
7.2.45, which is an expression for the ultimate size of the gas space
external to the bladder following a step change in pressure. From
Equation 2.2.3, from which the partial pressure of the propellant vapor
on the gas side of the bladder, p_v, was ignored it can be realized that
if the permeation rate for propellant molecules is not small compared
to that for the gas then the partial pressure driving force for pressurant
gas will be decreased. Equation 7.4.45 indicates that an increase in
propellant permeation rate over that expected by bladder-vapor measure-
ments would serve to reduce the gas space behind the bladder as predicted
by this equation. Data of this type to be used for design purposes
should, of course, be collected with the actual propellants and bladder
materials.

5.4   Effect of Hole Shape on Leakage Rate

The effect of the shape of the hole in the diffusion barrier was
investigated under Phase I of this study. It was found that when the
presence of the liquid was ignored the shape of the hole did not have a
strong influence on the leakage per unit area except for gross changes. For
example, a square hole and a circular hole of equal area resulted in a total
leakage rate through the structure which differed by only a few percent. On
the other hand, if the shape of the hole was radically altered,that is,
deformed from a square to a long narrow slit the effect on the leakage rate
per unit area was pronounced.

Including the liquid in the diffusion path will not alter this result
in any significant way. However, the updated Diffusion Analyzer Program has
the capability to predict the leakage rate through laminated bladder structures
with an arbitrary shaped hole in the barrier when both bubble formation and
uniform absorption of the diffusing gas into the liquid propellant occurs.
We have not, under this phase of the program, run cases where the holes have
other than circular shape because it appears that the results of Phase I on
this point are sufficiently conclusive.

5.5 Application to Estimating Quantity of Gas in Liquid Propellant for a Given Mission Profile

The results of the present study can be used to obtain useful information concerning the degree of pressurant gas contamination of liquid propellant for a given mission profile provided laminated bladder structure parameters such as Teflon and diffusion barrier thicknesses and approximate hole sizes and distributions are known. During this phase of the study, the presence of the liquid has been taken into account when estimating the leakage of pressurant gas into the liquid propellant. For example, Equation 4.1.1 can be used to obtain the level of pressurant gas contamination in a given bladder installation and for a given mission profile at any time during the mission. Examples are given in Figures 4.1-1 to 4.1-4 in which the quantity of pressurant gas dissolved in liquid propellant due to leakage through a circular hole in the metallic diffusion barrier is plotted according to Equation 4.1.1 for the pressurant gas propellant combinations

$$N_2 - N_2O_4$$

$$N_2 - N_2H_4$$

$$He - N_2O_4$$

$$He - N_2H_4$$
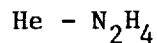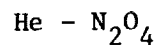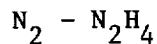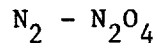
For a given level of pressurant gas pressure the quantity of pressurant gas dissolved uniformly in the liquid propellant can be obtained via Equation 4.1.1.

Based on the experimental evidence presented in this report, it seems that bubble formation on the liquid side of Teflon-metal foil-Teflon laminates, even with holes as large as 0.020" in diameter, is extremely unlikely, although tests should be performed on samples fabricated in the same manner as the bladder in question.

In Section 2.2 an expression for the growth rate of a gas bubble, assuming its existence, was derived and compared with the experimentally observed growth rates of various bubbles. While the essential elements of the growth phenomenon seem to be resonably modeled by this expression, the agreement with actual experimental values, using the permeation constants of He pressurant gas through Teflon determined during Phase I of this program, is only approximate.

However, differences of an order of magnitude or more are not uncommon in diffusion measurements (Reference 1) and, in addition, the bladder sample used during this phase of the study for the bubble growth tests was not from the same manufactured lot as that used in Phase I for the pressurant gas permeation measurements.

Additional experiments are required to more fully understand the mechanism by which gas bubbles can form on a Teflon bladder surface. It may then be possible to modify the surface condition of the Teflon, e.g. by heating the surface and slightly melting it, and to control the thermodynamic variables of pressure and temperature to minimize or eliminate the problem of gas bubble formation and growth on the liquid side of the bladder.

5.6 Further Problems

As a result of this study numerous problems associated with predicting leakage rate through laminated bladder structures having imperfect diffusion barriers have been overcome. We have measured the basic permeation parameters governing the diffusion of the common pressurant gases nitrogen and helium through FEP and TFE type Teflon and have obtained the data for N_2O_4 propellant vapor. In addition, the solubility and diffusivity of pressurant gases nitrogen and helium in the liquid propellants N_2O_4 and N_2H_4 have been measured. Finally, as a first step towards making the results applicable to space storable mild cryogenic propellants we have measured the binary diffusion coefficients of OF_2 and B_2H_6 vapors relative to the pressurant gases nitrogen and helium. To utilize this data considerable analytical capability has been developed. The problem of diffusion of a single component through circular holes in a sandwich shaped Teflon bladder structure was mathematically solved and under Phase II this problem was extended to include diffusion into the liquid. A generalized computer program was developed allowing the prediction of gas leakage rates through sandwich structures with an arbitrary shaped hole in the diffusion barrier and this program has been extended to include bubble growth on the liquid side of the bladder.

Although much progress has been made in solving the general problem, certain specific areas remain which are not well understood. For example, it has been observed that, under some circumstances, bubbles of gas are formed within the liquid during the process of pressurant gas transfer to the liquid propellant. The actual mechanism by which these bubbles are formed is not well understood and as a consequence we are unable to define the conditions under which they will or will not form. At the present time the weight of the evidence indicates that the bubbles grow from microvoids on the surface of the Teflon bladder. If this is the case, then it should be possible to develop bladder surfaces with a very low tendency to gas formation; however, other mechanisms are possible and we cannot state categorically at this time whether or not the above surmise is correct. It might even true that the formation and growth of bubbles is not even a problem with very low leakage rate bladder structures, for example, the Teflon-foil-Teflon bladder structure,

because the leakage rate is too slow to support the bubble growth. Under these circumstances a very small bubble would lose gas to the liquid more rapidly than it acquires gas through the teflon resulting in collapse rather than growth of the bubble. These questions which are of considerable importance to the national space program, unfortunately cannot be answered at the present time. However, a modest experimental and analytical program, if undertaken now, could provide the answers in the near future.

6.0 REFERENCES

1. "A Study to Analyze the Permeation of High Density Gases and Propellant Vapors Through Single Layer Teflon or Teflon Structure Materials and Laminations," TRW Interim Final Report Ph I, Contract NAS 7-505, 25 October, 1967.

2. Abramson, H. N., "The Dynamic Behavior of Liquids in Moving Containers," NASA SP-106, p. 395, 1966.

3. Landau, L. D. and Lifshitz, E. M., "Statistical Physics," Pergamon Press Ltd., London, 1958.

4. Zuber, N., "Hydrodynamic Aspects of Boiling Heat Transfer," Ph.D. Thesis, June 1959, University of California at Los Angeles, Department of Engineering.

5. Boardman, L. E. and Wild, N. E., Proc. Roy. Soc. (London) A 162, 511 (1937).

6. Coward, H. F. and Georgeson, E. H. M., J. Chem. Soc., 1085 (1937).

7. Westenberg, A. A. and Walker, R. E., J. Chem Phys., 29, 1139 (1958).

8. Giddings, J. F. and Seager, S. L., Ind. Eng. Chem. Fundamentals, 1, 277 (1962).

9. Walker, R. E. and Westenberg, A. A., J. Chem. Phys., 26, 1544 (1957).

10. Ibid, 31, 519 (1959).

11. Ibid, 32, 1314 (1960).

12. Seager, S. L., et. al., J. Chem. Eng. Data, 8, 168 (1963).

13. Fairbanks, D. F. and Wilke, C. R., Ind. Eng. Chem., 42, 471 (1950).

14. Kenmard, E. H., "Kinetic Theory of Gases," McGraw-Hill, New York (1938).

15. Gardner, M. P., et. al, "Study of Pressurant Gas Solubility in Nitrogen Tetroxide and Aerozine 50 - Chemistry Support of the LMDE 500Hz Program," Final Report, TRW No. 01827-6205-RO-00, 10 December, 1968.

16. Crank, J., "Mathematics of Diffusion," p. 273, Oxford Deredon Press, London (1956).

17. Stannett, V. and Yasuda, H., "Liquid Versus Vapor Permeation Through Polymer Films," Journal Polymer Science, No. 6, Part B, p. 289, 1963.

18. Thornton, E. R. et. al., "The Permeation of Vapors and Liquids Through Polymer Films," Journal Polymer Science, Vol. 28, p. 465, 1958.

19. Yasuda, H. and Stannett, V., Journal Polymer Science, Vol. 57, p. 907, 1958.

20. Sivadjian, J. and Riberio, D., "Permeability to Water and Water Vapor of Plastic Materials by the Hydrophotographic Technique," J. Appl. Poly. Sci., 8, No. 3, p. 1403, 1964.

21. Gradshteyn, I. S. and Ryzhik, I. M., "Table of Integrals, Series and Products," Academic Press, 1965.

7.0 APPENDICES

7.1 Leakage of Pressurant Gas Through a Laminated Bladder Structure Into a Body of Liquid Propellant

Consider a system consisting of a laminated bladder structure with a circular hole in the diffusion barrier, with pressurant gas at pressure P_o on one side, liquid propellant on the other. The steady state leakage rate of pressurant gas through the laminated structure (ignoring the liquid) was calculated during Phase I of this program for an arbitrary concentration difference across the bladder. The steady state leakage rate was found to have the form (Reference 1, p. 2-8)

$$W = f (P_1, P_2, a, b, h) \Delta c \qquad (7.1.1)$$

where f is a known function of the permeabilities of the Teflon layers P_1, P_2, the hole radius a, and the layer thicknesses, b and h. The quantity Δc is the concentration difference between the gas and liquid sides, that is

$$\Delta c = c_o - c_\ell \qquad (7.1.2)$$

where c_ℓ is the concentration on the liquid side of the bladder.

The direct extension of this analysis to transient leakage into a body of liquid is quite difficult but an approximate approach which should give good engineering results can be obtained in a relatively simple manner. This approach takes into account the fact that the lifetime of concentration transients in the bladder material are small compared to those in the liquid because the physical dimensions of that part of the bladder which takes part in the process is small compared to that of the body of the liquid propellant. As a result, processes in the bladder can be considered as quasi-steady and the leakage rate through the bladder structure calculated by equation 7.1.1 when account is taken of the change of c_ℓ with time. By coupling equation 7.1.1 with the concentration equation in the liquid, the time dependence of the leakage rate into the liquid can be obtained. This equation is

$$\frac{1}{D_\ell} \frac{\partial c}{\partial t} = \frac{\partial^2 c}{\partial x^2} \qquad (7.1.3)$$

where c is the mass fraction of pressurant gas in the liquid, D_ℓ is the diffusivity of the gas in the liquid and x is the coordinate normal to the bladder surface directed into the liquid.

Equation 7.1.3 is to be solved subject to the condition that the current into the liquid be given by equation 7.1.1, divided by the effective surface area, which was shown in Reference 1 to extend over about 10 hole radii. If there are many holes in the bladder, then W should be divided by the area of the bladder. In either case, the total leakage rate will be correct to within the accuracy of the analysis. Thus, we attempt to solve equation 7.1.3 subject to the condition that the current at x = 0, $j = -\rho_\ell D_\ell \frac{\partial c}{\partial x}$, equals $\frac{W}{A}$ where A is an appropriately chosen area. This can be done by Laplace Transform techniques as follows:

The transform of equation 7.1.3 is

$$\frac{s}{D_\ell} c(x,s) = \frac{d^2 c(x,s)}{dx^2} \tag{7.1.4}$$

which has solution, finite for large x,

$$c(x,s) = A(s) \, e^{-\sqrt{\frac{s}{D_\ell}} \, x} \tag{7.1.5}$$

The coefficient A(s) is determined from the condition at x = 0

$$\rho_\ell D_\ell \sqrt{\frac{s}{D_\ell}} A(s) = \frac{f}{A_e} \left\{ \frac{c_o}{s} - \frac{k_2}{k_\ell} c(o,s) \right\}$$

$$= \frac{f}{A_e} \frac{c_o}{s} - \frac{k_2}{k_\ell} \frac{f}{A_e} A(s)$$

Where A_e is the effective area of influence of the hole and where we have used the relation $\frac{c_\ell}{k_2} = \frac{c}{k_\ell}$ to eliminate c_ℓ.

$$A(s) = \frac{c_o}{s} \frac{k_\ell}{k_2} \frac{1}{1 + \frac{k_\ell \rho_\ell D_\ell A_e}{k_2 f} \sqrt{\frac{s}{D_\ell}}}$$

and

$$c(x,s) = \frac{c_o}{s} \frac{k_\ell}{k_2} \frac{e^{-\sqrt{\frac{s}{D_\ell}} \, x}}{1 + \sqrt{\alpha s}} \tag{7.1.6}$$
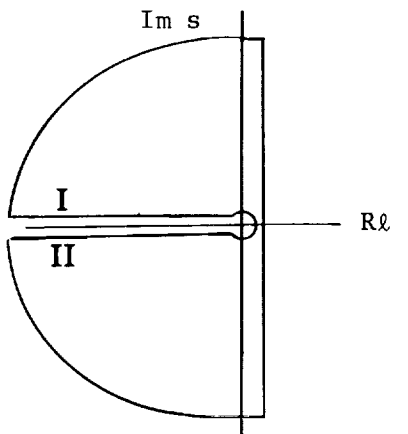
where

$$\alpha = \frac{k_\ell^2 \rho_\ell^2}{k_2^2 f^2} D_\ell A_e^2 .$$

By the Inversion Theorem for Laplace Transforms

$$\frac{k_2}{k_\ell} \frac{1}{c_o} c(x,t) = \frac{1}{2\pi i} \int_{\gamma - i\infty}^{\gamma + i\infty} \frac{e^{st - \sqrt{\frac{x^2}{D_\ell}} \sqrt{s}}}{1 + \sqrt{\alpha s}} \frac{ds}{s} \qquad (7.1.7)$$

The singularities of the integrand are a pole at the origin, s=0, and a branch point, also at s=0. The contour for evaluating the integral is shown below. Thus

$$\frac{1}{2\pi i} \int_{\gamma - i\infty}^{\gamma + i\infty} \frac{e^{st - \sqrt{\frac{x^2}{D_\ell}} \sqrt{s}}}{1 + \sqrt{\alpha s}} \frac{ds}{s} = 1$$

$$- \left(\frac{1}{2\pi i} \int_I (\quad) ds + \frac{1}{2\pi i} \int_{II} (\quad) ds \right) \qquad (7.1.8)$$

where the numerals I and II indicate the integration of the function over the paths I and II respectively. On I, $s = re^{i\pi}$ $ds = e^{i\pi} dr$ $\sqrt{s} = \sqrt{re}^{\ i\pi/2} = i\sqrt{r}$ while on II, $s = re^{-i\pi}$ $ds = e^{-i\pi} dr$ and $\sqrt{s} = \sqrt{r} e^{-i\pi/2} = -i\sqrt{r}$. Therefore,

$$\frac{1}{2\pi i} \int_I \frac{e^{st - \sqrt{\frac{x^2}{D_\ell}} \sqrt{r}}}{1 + \sqrt{\alpha s}} \frac{ds}{s} = \frac{1}{2\pi i} \int_\infty^0 \frac{e^{-rt - i\sqrt{\frac{x^2}{D_\ell}} \sqrt{r}}}{1 + i\sqrt{\alpha} \sqrt{r}} \frac{e^{i\pi} dr}{e^{i\pi} r} \quad \text{and}$$

$$\frac{1}{2\pi i} \int_{II} \frac{e^{st - \sqrt{\frac{x^2}{D_\ell}} \sqrt{r}}}{1 + \sqrt{\alpha s}} \frac{ds}{s} = \frac{1}{2\pi i} \int_o^\infty \frac{e^{-rt + i\sqrt{\frac{x^2}{D_\ell}} \sqrt{r}}}{1 - i\sqrt{\alpha} \sqrt{r}} \frac{e^{-i\pi} dr}{e^{-i\pi} r}$$

Substituting these relations in equation 7.1.8 we have

$$\frac{k_2}{k_\ell} \frac{1}{c_o} c(x,t) = 1 - \left\{ \frac{1}{2\pi i} \int_0^\infty \frac{e^{-rt+i\sqrt{\frac{x^2}{D_\ell}}\sqrt{r}}}{1 - i\sqrt{\alpha}\,\sqrt{r}} \frac{dr}{r} - \frac{1}{2\pi i} \int_0^\infty \frac{e^{-rt-i\sqrt{\frac{x^2}{D_\ell}}\sqrt{r}}}{1 + i\sqrt{\alpha}\,\sqrt{r}} \frac{dr}{r} \right\}$$

or

$$c(x,t) = \frac{k_\ell}{k_2} c_o - \frac{k_\ell}{k_2} c_o \left\{ \frac{1}{\pi} \int_0^\infty \frac{\sin\beta\sqrt{r}\;e^{-rt}}{(1+\alpha r)} \frac{dr}{r} + \frac{\sqrt{\alpha}}{\pi} \int_0^\infty \frac{\sqrt{r}\,\cos\beta\sqrt{r}\;e^{-rt}}{(1+\alpha r)} \frac{dr}{r} \right\}$$

where $\beta = \dfrac{x^2}{D} = \dfrac{x}{\sqrt{D_\ell}}$ The current at $x = 0$ is $-\rho_\ell D_\ell \dfrac{\partial c}{\partial x}\Big|_{x=0}$

and is given by

$$j(t) = \frac{\rho_\ell D_\ell}{\sqrt{D_\ell}} \frac{k_\ell}{k_2} c_o \frac{1}{\pi} \int_0^\infty \frac{e^{-rt}}{(1+\alpha r)} \frac{dr}{r^{1/2}} \qquad\qquad 7.1.9$$

Making the substitution $\alpha r = u^2$ reduces this equation to

$$j(t) = \frac{2fc_o}{\pi} \int_0^\infty \frac{e^{-\frac{t}{\alpha}u^2}}{1 + u^2}\,du \qquad\qquad 7.1.10$$

The last integral is known (21). Therefore,

$$j(t) = fc_o\,e^{\varepsilon t}\left[1 - \Phi(\sqrt{\varepsilon t}) \right] \qquad\qquad 7.1.11$$

where

$$\varepsilon = \frac{1}{\alpha} = \frac{k_2^2 f^2}{k_\ell^2 \rho_\ell^2 D_\ell A_e^2} \qquad \text{and}$$

$$\Phi(\sqrt{\varepsilon t}) = \frac{2}{\sqrt{\pi}} \int_0^{\sqrt{\varepsilon t}} e^{-\theta^2}\,d\theta$$

is the error function. The total leakage up to a given time T is obtained
by integrating equation 7.1.1

$$J(T) = \int_0^T j(t')dt' = fC_o \int_0^T e^{\epsilon t'}dt' - fC_o \int_0^T e^{\epsilon t'}\phi\left(\sqrt{\epsilon t'}\right)dt' \qquad (7.1.12)$$

The integration is straightforward and yields finally

$$\frac{J(T)}{c_o} = \frac{f}{\epsilon} e^{\epsilon T}\left(1 - \phi\left(\sqrt{\epsilon T}\right)\right) + \frac{4f}{\epsilon\sqrt{\pi}}\left(\sqrt{\epsilon T} - \frac{\sqrt{\pi}}{4}\right) \qquad (7.1.13)$$

for the total leakage rate to time T.

7.2 Detailed Analysis of the Effect of System Pressure Changes on a Volume of Gas on the Liquid Side of the Bladder.

Consider the configuration of Figure 7.1 below in which pressurant gas and propellant vapor are in thermodynamic equilibrium on both sides of a plane bladder. The final equilibrium volumes of the gas-vapor spaces after the addition of pressurant gas into space 1 is to be estimated in the following way. The whole process is divided into two parts, i.e., the bladder motion immediately after pressurization, and the motion due to the permeation of pressurant gas and propellant vapor across the bladder. In the first part, the mechanical response of the (frictionless) bladder to the increase in pressure is used to find the resulting volumes and partial pressures in each space. Diffusion during this phase is neglected since the time for the bladder to respond mechanically is much less than that required for the permeation of gas and vapor. For the second part of the analysis, the values of partial pressure and volume found in the first part are used as initial conditions for the determination of the motion of the bladder due to the permeation of pressurant gas and propellant vapor across the bladder.

Tank Wall   Bladder
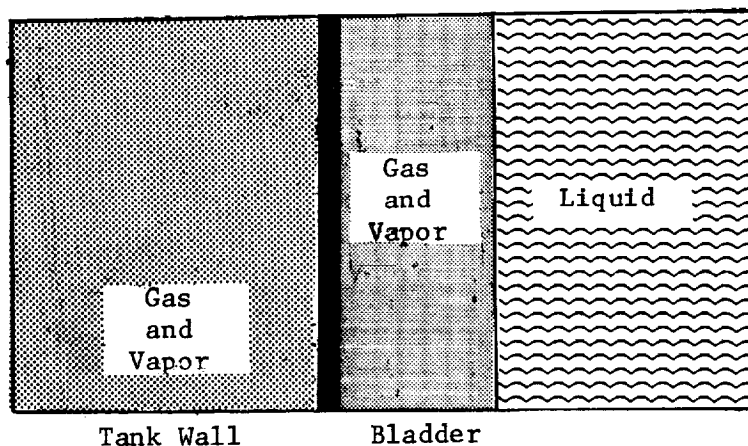
Figure 7.2-1 Illustrating System Geometry

The analysis is conducted as follows: Let subscript g denote quantities describing the state of the gas, subscript v the vapor, and let superscripts 1 and 2 refer to the gas and the gas vapor spaces respectively. We first calculate the changes in volumes and partial pressure brought about by the addition of pressurant gas. To do this we assume the gas and vapor obey the ideal gas laws. We also assume that the pressurization takes place

in a short enough period of time so that leakage of the gas into the liquid can be neglected during pressurization. Then

$$p_i^1 V_i^1 = n_i^1 RT \qquad (7.2.1)$$

where subscript i denotes initial values, and after gas injection,

$$p_f^1 V_f^1 = n_f^1 RT \qquad (7.2.2)$$

For space 2 we have two similar equations

$$p_i^2 V_i^2 = n_i^2 RT \qquad (7.2.3)$$

$$p_f^2 V_f^2 = n_f^2 RT \qquad (7.2.4)$$

Since $p_2^1 = p_i^2 = p_i$ and $p_f^2 = p_f^1 = p_f$ we have, upon dividing 7.2.4 by 7.2.2

$$\frac{V_f^2}{V_f^1} = \frac{n_f^2}{n_f^1} \qquad (7.2.5)$$

The number of moles finally on side 1, n_f^1, differs from n_2^1 by the number of moles of gas added, while n_f^2 differs from n_1^2 by the number of moles of propellant vapor condensed during the pressurization. Thus

$$n_f^2 = n_{gi}^2 + n_{vf}^2 \qquad (7.2.6)$$

where n_{gi}^2 is the number of moles of gas initially on the liquid side in volume 2 and n_{vf}^2 is the number of moles of vapor finally present there. The latter quantity can be calculated from the fact that the partial pressure of the vapor in volume 2 is equal to the liquid vapor pressure, $P_{v\ell}$. Thus

$$P_{v\ell} V_f^2 = n_{vf} RT \qquad (7.2.7)$$

and

$$n_f^2 = n_{gi}^2 + \frac{P_{v\ell}V_f^2}{RT} \tag{7.2.8}$$

Also n_{gi}^2 can be calculated from the initial pressure and volume.

$$n_{gi}^2 = \frac{p_{gi}^2 V_i^2}{RT} = \frac{(p_i - p_\ell)V_i^2}{RT} \tag{7.2.9}$$

Thus

$$n_f^2 = \frac{(p_i - p_{v\ell})V_i^2}{RT} + \frac{P_{v\ell}V_f^2}{RT} \tag{7.2.10}$$

and using these results in (7.2.5) gives

$$\frac{V_f^2}{V_f^1} = \frac{1}{RTn_f^1} \left\{ (p_i - p_{v\ell})V_i^2 + p_{v\ell}V_f^2 \right\} \tag{7.2.11}$$

or again using Equation (7.2.2)

$$V_f^2 = \frac{1}{p_f} \left\{ (p_i - p_{v\ell})V_i^2 + p_{v\ell}V_f^2 \right\} \tag{7.2.12}$$

Solving for V_f^2 we obtain

$$\frac{V_f^2}{V_i^2} = \frac{p_i - p_{v\ell}}{p_f - p_{v\ell}} \tag{7.2.13}$$

Since the total gas volume is constant (assuming the liquid is incompressible) the relation

$$V = V_f^1 + V_f^2 = V_i^1 + V_i^2 \tag{7.2.14}$$

7-8

must hold. Hence Equation (7.2.13) yields also the result.

$$\frac{V_f^1}{V_i^1} = \left(1 - \frac{p_i - p_{v\ell}}{p_f - p_{v\ell}}\right)\frac{V}{V_i^1} + \frac{p_i - p_{v\ell}}{p_f - p_{v\ell}} \qquad (7.2.15)$$

Note that if the vapor pressure is much less than than either p_i or p_f then $V_f^2/V_i^2 = p_i/p_f$ as expected.

We now calculate the new propellant vapor partial pressure on the gas side. We have

$$p_{vf}^1 V_f^1 = n_{vf}^1 RT \qquad (7.2.16)$$

But $n_{vf}^1 = n_{vi}^1$ since no vapor is added or leaks out of Volume 1 during the period of pressurization. Thus

$$p_{vf}^1 V_f^1 = n_{vi}^1 RT \qquad \text{and}$$

$$p_{vf}^1 = \frac{n_{vi}^1 RT}{V_f^1} \qquad (7.2.17)$$

Also $p_{vi}^1 = p_{v\ell}$ by hypothesis and $p_{v\ell} V_i^1 = n_{vi}^1 RT$ so

$$p_{vf}^1 = p_{vi} \frac{V_i^1}{V_f^1} = \frac{p_{v\ell}}{\left(1 - \dfrac{p_i - p_{v\ell}}{p_f - p_{v\ell}}\right)\dfrac{V}{V_i^1} + \dfrac{p_i - p_{v\ell}}{p_f - p_{v\ell}}} \qquad (7.2.18)$$

Since $V_f^1 > V_i^1$ the final vapor pressure is less than the initial vapor pressure so that no propellant is condensed. The initial driving force for the permeation of vapor from Volume 2 to Volume 1 is therefore not $p_{v\ell}$ but

$$p_{v\ell} - p_{vf}^1 = p_{v\ell}\left[1 - \frac{1}{\left(1 - \dfrac{p_i - p_{v\ell}}{p_f - p_{v\ell}}\right)\dfrac{V}{V_i^1} + \dfrac{p_i - p_{v\ell}}{p_f - p_{v\ell}}}\right] \qquad (7.2.19)$$

This is also the initial partial pressure differential for the permeation of gas from Volume 1 to Volume 2 since

$$p_f^1 = p_{gf}^1 + p_{vf}^1 = p_f^2 = p_{gf}^2 + P_{v\ell}$$

so that

$$P_{v\ell} - p_{vf}^1 = p_{gf}^1 - p_{gf}^2 \qquad (7.2.20)$$

We note that if $p_f \gg p_i$, (large system pressure increase) then

$$P_{v\ell} - p_{vf}^1 = p_{gf}^1 - p_{gf}^2 = P_{v\ell}\left(1 - \frac{v_i^1}{v}\right) \qquad (7.2.21)$$

and the initial driving force depends on the ratio of the initial gas volume (Volume 1) to the total volume $V_i^1 + V_i^2$. Thus the driving force will be the larger when the volume V_i^2 on the liquid side is largest.

The system is now no longer in total thermodynamic equilibrium after the increase in system pressure. The partial pressures of each component differ on each side of the permeable membrane and counter permeation of the propellant vapor and gas results. The system will ultimately reach equilibrium again with new values of V^1 and V^2. By comparing these final values with the initial values V_i^1 and V_i^2 we can determine the overall change in system configuration which results from the pressurization. In this way we can determine if there is a net increase in the quantity of gas on the liquid side as a result of the process of pressurizing the tank in the presence of a gas volume on the liquid side.

Assuming that the permeation process is sufficiently slow to justify the neglect of concentration transients in the membrane material we can write the following first order equations for the number of moles of vapor and gas present on each side of the bladder as a function of time after the termination of the pressurization process.

o   Number of moles of vapor in Volume 1

$$\frac{dn_v^1(t)}{dt} = \frac{P_v A}{\ell} \left(p_{v\ell} - p_v^1(t) \right) \qquad (7.2.22)$$

o Number of moles of gas in Volume 1

$$- \frac{dn_g^1(t)}{dt} = \frac{P_g A}{\ell} \left(p_g^1(t) - p_g^2(t) \right) \qquad (7.2.23)$$

o Number of moles of gas in Volume 2

$$\frac{dn_g^2}{dt} = \frac{P_g A}{\ell} \left(p_g^1(t) - p_g^2(t) \right) - L(t) \qquad (7.2.24)$$

where A is the bladder area, ℓ its thickness, P_g the gas and p_v the vapor permeabilities. L(t) is the leakage rate by diffusion of the pressurant gas into the liquid from Volume 2.

o Subsidiary relations

Mechanical Equilibrium $p^1(t) = p^2(t)$

$$p_g^1 + p_v^1 = p_g^2 + p_{v\ell}$$

Constant Total Volume $v^1(t) + v^2(t) = V = \text{constant}$

Ideal Gas Laws $p_g^1 v^1(t) = n_g^1 RT$

$$p_v^1 v^1(t) = n_v^1 RT$$

$$p_g^2 v^2(t) = n_g^2 RT$$

$$p_{v\ell} v^2(t) = n_v^2 RT$$

The unknowns in this system of equations are n_v^1, n_g^1, n_g^2, n_v^2, p_g^1, p_g^2, p_v^1, v^1 and v^2, a total of 9. There is a total of 9 relations among the variables so that the system is determinant.

Using the gas laws we eliminate n_v^1, n_g^1, and n_g^2 from Equations (7.2.22), (7.2.23) and (7.2.24) obtaining

$$\frac{1}{RT} \frac{d}{dt} \left[p_v^1 v^1(t) \right] = \frac{P_v A}{\ell} \left(P_{v\ell} - p_v^1 \right) \tag{7.2.25}$$

$$-\frac{1}{RT} \frac{d}{dt} \left[p_g^1 v^1(t) \right] = \frac{P_g A}{\ell} \left(p_g^1 - p_g^2 \right) \tag{7.2.26}$$

$$\frac{1}{RT} \frac{d}{dt} \left[p_g^2 v^2(t) \right] = \frac{P_g A}{\ell} \left(p_g^1 - p_g^2 \right) - L(t). \tag{7.2.27}$$

Eliminating p_v^1 and $V^2(t)$ by use of the relations

$$p_v^1 = P_{v\ell} - \left(p_g^1 - p_g^2 \right)$$

$$v^2(t) = V - v^1(t)$$

we obtain the following three equations in three unknowns.

$$\frac{1}{RT} \frac{d}{dt} \left\{ \left[P_{v\ell} - \left(p_g^1 - p_g^2 \right) \right] v^1(t) \right\} = \frac{P_v A}{\ell} \left(p_g^1 - p_g^2 \right) \tag{7.2.28}$$

$$\frac{1}{RT} \frac{d}{dt} \left[p_g^1 v^1(t) \right] = -\frac{P_g A}{\ell} \left(p_g^1 - p_g^2 \right) \tag{7.2.29}$$

$$\frac{1}{RT} \frac{d}{dt} \left[p_g^1 \left(V - v^1(t) \right) \right] = \frac{P_g A}{\ell} \left(p_g^1 - p_g^2 \right) - L(t) \tag{7.2.30}$$

The function $L(t)$ depends only on the difference $\left(p_g^2(t) - p_{gi}^2 \right)$ and on the diffusivity and solubility of the pressurant gas in the liquid propellant. Thus the above equations contain only the unknowns $p_g^1(t)$, $p_g^2(t)$ and $v^1(t)$. A general solution is, however, quite difficult to obtain since the equations are not linear. It is easy, however, to obtain one general integral of these equations the results of which suffice to calculate the final value of $v^1(t)$, the quantity of most interest.

By dividing Equation (7.2.28) by (7.2.29) and rearranging we obtain the result

$$\frac{1}{V^1(t)} \frac{dV^1}{dt} = - \frac{1}{\left[P_{v\ell} + p_g^2 - p_g^1\left(1 - \frac{P_v}{P_g}\right)\right]} \frac{d}{dt}\left[P_{v\ell} + p_g^2 - p_g^1\left(1 - \frac{P_v}{P_g}\right)\right]$$

(7.2.31)

which has the integral

$$\frac{V^1(t)}{V^1(0)} = \frac{P_{v\ell} + p_g^2(0) - p_g^1(0) + p_g^1(0)\dfrac{P_v}{P_g}}{P_{v\ell} + p_g^2(t) - p_g^1(t) + p_g^1(t)\dfrac{P_v}{P_g}}$$

(7.2.32)

In the limit of large t when the system once again reaches equilibrium we have $p_g^2(t) - p_g^1(t) = 0$ and

$$\frac{V^1(\infty)}{V^1(0)} = \frac{P_{v\ell} + p_g^2(0) - p_g^1(0) + p_g^1(0)\dfrac{P_v}{P_g}}{P_{v\ell} + p_g^1(\infty)\dfrac{P_v}{P_g}}$$

(7.2.33)

Thus the final value of $V^1(t)$ can be found if we can obtain the values of the quantities on the right hand side of this equation. Note that the values here denoted as belonging to zero time are the previously calculated quantities denoted by subscript f for final, i.e., after the pressurization. In terms of this notation Equation (7.2.33) reads

$$\frac{V^1(\infty)}{V^1_f} = \frac{P_{v\ell} + p_{gf}^2 - p_{gf}^1 + p_{gf}^1\dfrac{P_v}{P_g}}{P_{v\ell} + p_g^1(\infty)\dfrac{P_v}{P_g}}$$

(7.2.34)

This equation can be somewhat simplified by noting that $P_{v\ell} + p_{gf}^2 - p_{gf}^1 = p_{vf}^1$ and that $p_{gf}^1 = P_f - p_{vf}^1$ as that Equation (7.2.34) becomes

$$\frac{V^1(\infty)}{V^1_f} = \frac{\dfrac{P_v}{P_g} p_f + \left(1 - \dfrac{P_v}{P_g}\right) p^1_{vf}}{p_{v\ell} + p^1_g(\infty) \dfrac{P_v}{P_g}} \tag{7.2.35}$$

We have p^1_{vf} from Equation (18) so that we only need to calculate $p^1_g(\infty) = p^2_g(\infty) = p_g(\infty)$. This quantity depends on the number of moles of gas dissolved in the propellant. It is given by

$$p_g(\infty)V = n_g(\infty)RT \tag{7.2.36}$$

where $n_g(\infty)$ is the total number of moles of gas left in the system exclusive of that dissolved in the liquid. The quantity dissolved in the liquid is

$$\Delta n_g = k_\ell (p_g(\infty) - p_{gi}) V_\ell \tag{7.2.37}$$

where k_ℓ is the Henry law solubility and V_ℓ is the liquid propellant volume. Thus

$$p_g(\infty)V = \left[n_{gf} - k_\ell (p_g(\infty) - p_{gi}) V_\ell \right] RT \tag{7.2.38}$$

and

$$p_g(\infty) = \frac{n_{gf}RT + k_\ell (p_i - p_{v\ell}) V_\ell RT}{V + k_\ell V_\ell RT} \tag{7.2.39}$$

The quantity n_{gf} can be obtained from the gas laws. Thus

$$p^1_{gf} V^1_f = n^1_{gf} RT$$

$$p^2_{gf} V^2_f = n^2_{gf} RT$$

and
$$p^1_{gf} V^1_f + p^2_{gf} V^2_f = \left(n^1_{gf} + n^2_{gf} \right) RT = n_{gf} RT \tag{7.2.40}$$

Using $p_{gf}^1 = p_f - p_{vf}^1$; $p_{gf}^2 = p_f - p_{v\ell}$ we obtain

$$p_f V - p_{vf}^1 V_f^1 - p_{v\ell} V_f^2 = n_{gf} RT \qquad (7.2.41)$$

If the pressure to which the system is raised is considerably greater than the vapor pressure then it is sufficient to use

$$p_f V = n_{gf} RT \qquad (7.2.42)$$

so that Equation (7.2.39) becomes

$$p_g(\infty) = \frac{p_f V + k_\ell (p_i - p_{v\ell}) V_\ell RT}{V + k_\ell V_\ell RT}$$

or

$$p_g(\infty) = p_f \left(\frac{1 + k_\ell \dfrac{V_\ell}{V} RT \dfrac{(p_i - p_{v\ell})}{p_f}}{1 + k_\ell \dfrac{V_\ell}{V} RT} \right) \qquad (7.2.43)$$

We now have all the quantities necessary to evaluate $V^1(\infty)$ in terms of known parameters. Note that from Equation (7.2.15)

$$V_f^1 = \left(1 - \frac{p_i - p_{v\ell}}{p_f - p_{v\ell}} \right) V + \left(\frac{p_i - p_{v\ell}}{p_f - p_{v\ell}} \right) V_i^1 \qquad (7.2.44)$$

and p_{vf}^1 is given by Equation (7.2.18). Combining Equations (7.2.43), (7.2.44), (7.2.18) and (7.2.35) we obtain

$$\frac{V^1(\infty)}{\left(1 - \dfrac{p_i - p_{v\ell}}{p_f - p_{v\ell}}\right)V + \left(\dfrac{p_i - p_{v\ell}}{p_f - p_{v\ell}}\right)V_i^1}$$

$$= \frac{\dfrac{P_v}{P_g}\, p_f + \left(1 - \dfrac{P_v}{P_g}\right)\left[\dfrac{p_{v\ell}}{\left(1 - \dfrac{p_i - p_{v\ell}}{p_f - p_{v\ell}}\right)\dfrac{V}{V_i^1} + \dfrac{p_i - p_{v\ell}}{p_f - p_{v\ell}}}\right]}{p_{v\ell} + \dfrac{P_v}{P_g}\, p_f\left[\dfrac{1 + k_\ell\, \dfrac{V_\ell}{V}\, RT\, \dfrac{(p_i - p_{v\ell})}{p_f}}{1 + k_\ell\, \dfrac{V_\ell}{V}\, RT}\right]} \qquad (7.2.45)$$

Using Equation (7.2.45) we can calculate $V^1(\infty)$ for various values of P_f, P_i, V, V and V_1^1.

7.3   Theoretical Estimates of Gas-Vapor Diffusion Coefficients

In order to more realistically analyze the problem of pressurant gas disposition on the propellant side of a bladder, the binary diffusion coefficients of various pressurant gas-propellant vapors are required. The gas-vapor combinations of interest here are:

$$He - N_2H_4 \qquad\qquad N_2 - N_2H_4$$

$$He - N_2O_4 \qquad\qquad N_2 - N_2O_4$$

$$He - B_2H_6 \qquad\qquad N_2 - B_2H_6$$

$$He - OF_2 \qquad\qquad N_2 - OF_2$$
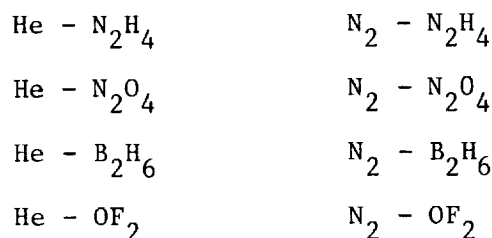
The binary diffusion coefficients of the above combinations can be calculated using the kinetic theory of gases.

Employing an analysis of the type initiated by Maxwell and Chapman (Ref.14), we regard the modification of the velocity distribution function of each gas species as the other species diffuses into it. Consider the balance of molecules in a volume element. The net flow of molecules, of say, gas i across unit area of the plane A in the unit time is due to that component of the molecular velocity perpendicular to plane A and is

$$\Sigma V_{ix} n_i$$

where V_{ix} is the molecular velocity in the x direction and n_i is the number of molecules of gas i per unit volume. The sum is over all molecules in unit volume in velocity space. This mass flux is equal to the product of the binary diffusion coefficient times the concentration gradient in the same direction (from gas i into gas j), or

$$D_{ij} \frac{dn_i}{dX} = \Sigma V_{ix} n_i \tag{7.3.1}$$

The volume sum in (7.3.1) can also be written as an integral in velocity space,

$$\sum V_{ix} n_i = n_i \int V_{ix} f_i(v_i) dk_i; \quad v_i = V_{ix}\hat{i} + V_{iy}\hat{j} + v_{iz}\hat{k} \tag{7.3.2}$$

where: $f_i(v)$ = the velocity distribution function, i.e., the fraction of molecules "i" whose velocity is within $dV_{ix}dV_{iz}$ of V_i, and

$$dk = dV_{ix} + dV_{iy} + dV_{iz}.$$

The method of Maxwell and Chapman consists, basically, of finding the modified form of $f_i(v_i)$ which occurs due to the mass concentration gradient present in the system and substituting it into (7.3.2) to calculate the value of $\Sigma v_{ix} n_i$. The binary diffusion coefficient for gas i diffusing into j, D_{ij}, is then obtainable from (7.3.1). As will be seen at the end of the development, the expression for D_{ij} is symmetric in subscripts i and j for dilute concentration and, hence, the binary diffusion coefficient for gas i in gas j is identical with gas j in gas i.

The distribution function for a specific type of molecule is assumed to be of the form

$$f_i = f_{oi} + f_{si} \tag{7.3.3}$$

where: $f_{oi} = A_i e^{-\beta_i^2 v_i^2}$ is the Maxwellian contribution and f_{si} is the small disturbance in the distribution function due to the diffusion of molecules of species i into the region occupied by species j. The form of f_{si} is determined by the differential Equation (7.3.4) below, (the modified Boltzman Equation) which describes the change in the number of molecules in steady state occupying a given volume in velocity and position space under the effects of molecular collisions and mass convection in one direction only.

$$V_{ix} \frac{\partial (n_i f_i)}{\partial X} = \left[\frac{\partial (n_i f_i)}{\partial t} \right]_{\text{collisions}} \tag{7.3.4}$$

Using (7.3.3) and (7.3.4) there results

$$V_{ix} \frac{\partial (n_i f_{oi})}{\partial X} + V_{ix} \frac{\partial (n_i f_{si})}{\partial X} = \left[\frac{\partial (n_i f_{oi})}{\partial t} \right]_{\text{coll.}} + \left[\frac{\partial (n_i f_{si})}{\partial t} \right]_{\text{coll.}} \tag{7.3.5}$$

Since f_{si} is small (same order as the concentration gradient) its derivative with respect to x will be smaller still. In addition, since the collisions can have no effect on the total number of molecules or, because of conservation of energy, on the quantity f_{oi}, (7.3.5) becomes

$$\left[\frac{\partial (n_i f_{si})}{\partial t} \right]_{coll.} = V_{ix} \frac{\partial (n_i f_{oi})}{\partial X}$$

Inserting the expression for f_{oi} there results

$$\left[\frac{\partial (n_i f_{si})}{\partial t} \right]_{coll.} = V_{ix} \left[A_i \frac{dn_i}{dX} + n_i \frac{dA_i}{dX} - n_i A_i^2 v_i^2 \frac{d\beta_i^2}{dX} \right] e^{-\beta_i^2 v_i^2} \qquad (7.3.6)$$

Since $\beta_i^2 = \frac{1}{2RT}$ and $A = \frac{\beta}{\pi^{3/2}}$ the derivatives involving these quantities appearing on the right hand of (7.3.6) and

$$\frac{d\beta_i^2}{dX} = - \frac{\beta_i^2}{T} \frac{dT}{dX} \qquad (7.3.7)$$

$$\frac{dA}{dX} = - \frac{3}{2} \frac{A}{\beta_i^2} \frac{d\beta_i^2}{dX} \qquad (7.3.8)$$

Inserting these into (7.3.6) results in

$$\left[\frac{\partial (n_i f_{si})}{\partial t} \right]_{coll.} = V_{ix} e^{-\beta_i^2 v_i^2} \left[A_i \frac{dn_i}{dX} + n_i \frac{3}{2} \frac{A}{T} \frac{dT}{dX} + n_i A_i v_i^2 \frac{\beta_i^2}{T} \frac{dT}{dX} \right] \qquad (7.3.9)$$

Since we are assuming the temperature is constant, $\frac{dT}{dX} = 0$ and (7.3.9) becomes

$$\left[\frac{\partial (n_i f_{si})}{\partial t} \right]_{coll.} = V_{ix} A_i e^{-\beta_i^2 v_i^2} \frac{dn_i}{dX} \qquad (7.3.10)$$

Since collisions do not change the number of molecules of species "i" present Equation (7.3.10) suggests the form for f_{si} of

$$f_{si} = C_i V_{ix} e^{-\beta_i^2 v_i^2} \qquad (7.3.11)$$

where C_i is a function of n_i and β_i

Having the modified velocity distribution function for the ith species due to the diffusion process, the volume sum of Equation (7.3.2) can be evaluated

$$V_{1x}n_i = n_i \int V_{1x}f_i(V_i) \, dk_i \qquad (7.3.12)$$

where, as before, $\Sigma V_{1x}n_i$ represents the net flow of molecules of species i across a unit plane. Substituting (7.3.11) for f_1 (since f_{oi} the Maxwellian contribution, is symmetric about $V_i = 0$) there results an integral

$$I = n_i C_i \iiint_{-\infty}^{\infty} V_{1x}^2 e^{-\beta_i^2 \left[V_{1x}^2 + V_{1y}^2 + V_{1z}^2 \right]} dV_{1x} dV_{1y} dV_{1z}$$

This integral is of known form, and its value is tabulated (cf. Kennard, p. 477)

$$I = \frac{\pi^{3/2} n_i C_i}{2\beta_i^5}$$

and therefore $\qquad \Sigma V_{1x}n_i = \frac{\pi^{3/2} n_i C_i}{2\beta_i^5} \qquad (7.3.13)$

The next problem is to determine the C_i. The gases are assumed to diffuse into each other with no gross convective motion. Therefore, the net flow of molecules of species 1 across a unit plane must be the same as that of species 2 across the same plane (in the opposite direction). Thus,

$$\Sigma V_{1x \, 1} = - \Sigma V_{2x}n_2$$

Substituting the expression calculated from the modified velocity distribution function for these volume (in velocity space) sums results in an expression which involves C_1 and C_2

$$\frac{C_1}{C_2} = - \frac{\beta_1^5 n_2}{\beta_2^5 n_1} \qquad (7.3.14)$$

where now C_1 and C_2 must be chosen such that f_{si} satisfies, to the best approximation, Equation (7.3.10). Following Chapman we multiply (7.3.10) by the transport function whose sum yields the net transfer of mass by diffusion, i.e. $V_{ix\ i}$, and integrate over the velocity space.

$$\int V_{ix} \left[\frac{\partial (n_i f_{si})}{\partial t} \right]_{coll.} dk = \int V_{ix}^2 A_i e^{-\beta i^2 V_i^2} \frac{dn_i}{dX} dk \qquad (7.3.15)$$

The physical significance of the left hand side of (7.3.15) can now be used to handle its evaluation. Taking the time differentiation outside the integral sign and recalling that molecules of species i are neither created nor destroyed as the result of molecular collisions the left hand integral of (7.3.15) becomes

$$\left[\frac{d}{dt} \right]_{coll.} \int V_{ik} f_{si} n_i dk$$

which is, by definition of the velocity distribution function f_{si}, also equal to

$$\left[\frac{d}{dt} \right]_{coll.} \Sigma V_{ix} n_i \qquad (7.3.16)$$

where the sum is over the velocity space. The expression (7.3.16) is the time rate of change of molecular diffusion across unit area due to collisions. It can also be written as

$$D_{ij} \Sigma V_{ix} n_i = \left[\frac{d}{dt} \right]_{coll.} \Sigma V_{ix} n_i \qquad (7.3.17)$$

where D_{ij} has the units of L^2/T. The rate of change of molecular diffusion across unit area in steady state is then given by Equations (7.3.15), (7.3.16) and (7.3.17)

$$D_{ij} \Sigma V_{ix} n_i = A_i \int V_{ix}^2 e^{-\beta_i^2 V_i^2} \frac{dn_i}{dX} dk \qquad (7.3.18)$$

The triple integral above is of the same form as that in Equation (7.3.12) Using its tabulated value and the expression for A_i there results

$$D_{ij} \Sigma V_{ix} n_i = \frac{1}{2\beta_i^2} \frac{dn_i}{dX}$$

(7.3.19)

It now remains to calculate $D_{ij} \Sigma V_{ix} n_i$ by considering directly the effect of collisions on $\Sigma V_{ix} n_i$. This calculation of the Maxwell-Chapman method though not difficult is extremely long and laborious and so will not be reproduced here. The result is (cf. Reference 14)

$$D_{ij} \Sigma V_{ix} n_i = -\frac{4}{3} \sqrt{\mu_j} \, \pi n_i n C_i \frac{S_d}{\beta_i^6}$$

(7.3.20)

where S_d is the collision cross section of the molecules (of the two species i and j), equal for spherical molecules to

$$S_d = \frac{\pi (d_i + d_j)}{4}$$

where d_1 and d_2 are the diameters of the spheres, $\mu_j = M_j/(M_i + M_j)$, and M_i being the gm-molecular weight; n_i and n are the number of molecules of gas; and gas i plus gas j per unit volume, respectively. Dividing (7.3.20) by Equation (7.3.15), C_i can be eliminated.

$$\frac{D_{ij} \Sigma V_{ix} n_i}{\Sigma V_{ix} n_i} = -\frac{8}{3} \sqrt{\mu_j} \frac{n S_d}{\pi^{1/2} \beta_i}$$

Substituting for $D_{ij} \Sigma V_{ix} n_i$ from Equation (7.3.19) and for $\Sigma_{ix} n_i$ from Equation (7.3.1) there results

$$D_{ij} = \frac{3}{8} \frac{1}{\sqrt{\mu_j}} \frac{\pi^{1/2} \beta_i}{n \, 2\beta_i^2 S_d}$$

(7.3.21)

Since the distribution function exponent and T, R, M are related by

$$\beta_i = \left(\frac{M_i}{2RT}\right)^{1/2}$$

Equation (7.3.21) can be rewritten as

$$D_{ij} = \frac{3}{8} \frac{1}{nS_d} \sqrt{\frac{\pi}{2}} \left[\frac{(M_i + M_j)}{M_i M_j} RT\right]^{1/2} \qquad (7.3.22)$$

which is symmetric in species i and j. The binary diffusion coefficient of gas i diffusing into gas j is therefore identical with that for gas j diffusing into gas i.

The method used here for determining S_d, the only unknown term in Equation (7.3.22) is as follows. For a given gas one of the other transport properties (thermal conductivity or viscosity) must be known. An analysis similar to that above leads to relations which yield thermal conductivity (or viscosity) as a function of other known physical properties and the diameter of an equivalent spherical molecule. These relations for thermal conductivity and viscosity, respectively, are

$$K_i = \frac{\rho_i \; 1.15 C_{vi} (3R_i T)^{1/2}}{\sqrt{2} \; \pi \eta_o d_i^2} \qquad (7.3.23)$$

and

$$\eta_i = \frac{\rho_i \; 0.46 \; (3R_i T)^{1/2}}{\sqrt{2} \; \pi \eta_o d_i^2} \qquad (7.3.24)$$

where: ρ_i, C_{vi}, R_i are the density, heat capacity at constant volume and gas constant for gas i. T is the temperature and η_o is the number of molecules of any perfect gas in one cubic centimeter at standard conditions ($\eta_o = 2.58 \times 10^{19}$ molecules/cm^3). The term d_i is the spherical diameter of an equivalent spherical molecule.

Equation (7.3.23) or (7.3.24) is used to determine an equivalent spherical molecular diameter, d_i, at the temperature of interest from thermal conducivity data of Table 3.1-1. Equivalent diameters found in this way for each species of

diffusion gas are used to determine the equivalent cross section for diffusion, S_d,

$$S_d = \frac{\pi \left(d_1^2 + d_2^2 \right)}{4} \qquad (7.3.25)$$

The diffusion coefficient of the two species can then be determined from Equation (7.3.22).

This approach was used to determine the binary diffusion coefficients of the pressurant gas-propellant vapor pairs itemized in the beginning of this section. These values are presented in Table 3.4 below where they are compared with the experimental values. The agreement is generally good.

TABLE 7.3-1

BINARY DIFFUSION COEFFICIENTS - A COMPARISON
BETWEEN CALCULATED AND EXPERIMENTAL RESULTS

	N_2O_4 (27°C)	N_2H_4 (77°C)	B_2H_6 (27°C)	OF_2 (27°C)
He	0.740 (exp)	0.630 (exp)	0.451 (exp)	0.600 (exp)
	0.567 (calc)	0.555 (calc)	0.430 (calc)	0.440 (calc)
N_2	0.348 (exp)	0.540 (exp)	0.270 (exp)	0.142 (exp)
	0.185 (calc)	0.204 (calc)	0.160 (calc)	0.150 (calc)

THIS IS THE MASTER LIST. DO NOT DELETE ANY OF THE NASA OR DOD
ORGANIZATIONS OR NAMES, ALTHOUGH ADDITIONAL ONES MAY BE ADDED.
ADDITIONAL INDUSTRY ORGANIZATIONS OR NAMES MAY BE ADDED BUT
DON,T DELETE EXISTING NAMES FOR ANY PARTICULAR COMPANY.
REPORT IS TO BE SENT DIRECTLY TO THE -RECIPIENTS- MARKED WITH AN -X-
UNDER THE COLUMN HEADED -DESIGNEE- (FIRST SECTION ONLY). IN
FOLLOWING SECTIONS, THE REPORT SHOULD BE SENT TO THE TECHNICAL
LIBRARIAN OF THE -RECIPIENT- WITH A CARBON COPY OF THE LETTER OF
TRANSMITTAL TO THE ATTENTION OF THE PERSON NAMED UNDER THE COLUMN
DESIGNEE. THE LETTER OF TRANSMITTAL SHOULD CONTAIN THE CONTRACT
NUMBER AND COMPLETE TITLE OF THE FINAL REPORT.

THE DISTRIBUTION LIST SHOULD BE INCLUDED IN THE FINAL REPORT AS AN
APPENDIX.

DISTRIBUTION LIST FOR FINAL REPORT

CONTRACT NAS7-505

COPIES	RECIPIENT	DESIGNEE
4	CHIEF, LIQ. PROP. TECHNOLOGY, RPL NASA WASHINGTON, D. C. 20546	(X)
1	DIRECTOR , LAUNCH VEHICLES AND PROPULSION , SV NASA WASHINGTON , D. C. 20546	(X)
1	DIRECTOR, ADVANCED MANNED MISSIONS, MT NASA WASHINGTON , D. C. 20546	.(X)
1	DIRECTOR , MISSION ANALYSIS DIVISION NASA AMES RESEARCH CENTER MOFFETT FIELD, CALIFORNIA 24035	(X)
	JET PROPULSION LABORATORY 4800 OAK GROVE DR. PASADENA , CALIF. 91103	
2	MR. DONALD L. YOUNG	(X)
	NASA PASADENA OFFICE 4800 OAK GROVE DRIVE PASADENA, CALIFORNIA 91103	
1	CONTRACTING OFFICER	(X)
1	OFFICE OF TECHNICAL INFORMATION AND PATENT MATTERS	(X)

25	NASA SCIENTIFIC + TECHNICAL INFORMATION FACILITY	(X)
	P. O. BOX 33	
	COLLEGE PARK, MARYLAND 20740	

	MARSHALL SPACE FLIGHT CENTER	
	HUNTSVILLE , ALABAMA , 35812	
1	MR. KEITH CHANDLER	(X)

NASA FIELD CENTERS

2	AMES RESEARCH CENTER MOFFETT FIELD, CALIFORNIA 94035	HAROLD HORNBY
2	GODDARD SPACE FLIGHT CENTER GREENBELT, MARYLAND 20771	MERLAND L. MOSESON CODE 620
2	JET PROPULSION LABORATORY CALIFORNIA INSTITUTE OF TECHNOLOGY 4800 OAK GROVE DRIVE PASADENA, CALIFORNIA 91103	HENRY BURLAGE, JR. PROPULSION DIV.
2	LANGLEY RESEARCH CENTER LANGLEY STATION HAMPTON, VIRGINIA 23365	DR. FLOYD L. THOMPSON DIRECTOR
2	LEWIS RESEARCH CENTER 21000 BROOKPARK ROAD CLEVELAND, OHIO 44135	DR. ABE SILVERSTEIN DIRECTOR
2	MARSHALL SPACE FLIGHT CENTER HUNTSVILLE, ALABAMA 35812	HANS G. PAUL CODE R-P+VFD WERNER VOSS R-P AND VE-PM
2	MANNED SPACECRAFT CENTER HOUSTON, TEXAS 77001	DR. ROBERT R. GILRUTH DIRECTOR G. THIBODAUX
2	WESTERN SUPPORT OFFICE 150 PICO BOULEVARD SANTA MONICA, CALIFORNIA 90406	ROBERT W. KAMM DIRECTOR
2	JOHN F. KENNEDY SPACE CENTER, NASA COCOA BEACH, FLORIDA 32931	DR. KURT H. DEBUS
1	NASA TEST FACILITY PROPULSION ENGINEERING OFFICE WHITE SANDS, NEW MEXICO	I.D. SMITH STAFF CHEMIST

GOVERNMENT INSTALLATIONS

1	AERONAUTICAL SYSTEMS DIVISION AIR FORCE SYSTEMS COMMAND WRIGHT-PATTERSON AIR FORCE BASE DAYTON, OHIO 45433	D.L. SCHMIDT CODE ASRCNC-2
1	AIR FORCE MISSILE DEVELOPMENT CENTER HOLLOMAN AIR FORCE BASE NEW MEXICO 88330	MAJ. R.E. BRACKEN CODE MDGRT
1	AIR FORCE MISSILE TEST CENTER PATRICK AIR FORCE BASE, FLORIDA	L.J. ULLIAN
1	AIR FORCE SYSTEMS DIVISION AIR FORCE UNIT POST OFFICE LOS ANGELES 45, CALIFORNIA 90045	COL. CLARK TECHNICAL DATA CENTER
2	AFFTC (FTBPP-2) EDWARDS AFB, CALIFORNIA 93523	MYRTLE C. JONES
1	ARNOLD ENGINEERING DEVELOPMENT CENTER ARNOLD AIR FORCE STATION TULLAHOMA, TENNESSEE 37388	DR. H.K. DOETSCH
1	BUREAU OF NAVAL WEAPONS DEPARTMENT OF THE NAVY WASHINGTON , D. C. 20546	J. KAY RTMS-41
1	DEFENSE DOCUMENTATION CENTER HEADQUARTERS CAMERON STATION, BUILDING 5 5010 DUKE STREET ALEXANDRIA, VIRGINIA 22314 ATTN- TISIA	
1	HEADQUARTERS, U.S. AIR FORCE WASHINGTCN 25, D.C. 20546	COL.C.K. STAMBAUGH AFRST

1	PICATINNY ARSENAL
	DOVER, NEW JERSEY 07801
		I. FORSTEN, CHIEF
		LIQUID PROPULSION
		  LABORATORY,
		  SMUPA-DL

2	AIR FORCE ROCKET PROPULSION LABORATORY RESEARCH AND TECHNOLOGY DIVISION AIR FORCE SYSTEMS COMMAND EDWARDS, CALIFORNIA 93523	RPRR/MR. H. MAIN
1	U.S. ATOMIC ENERGY COMMISSION TECHNICAL INFORMATION SERVICES BOX 62 OAK RIDGE, TENNESSEE 37830	A. P. HUBER OAK RIDGE GASEOUS DIFFUSION PLANT (ORGDP) P.O.BOX P
1	U.S. ARMY MISSILE COMMAND REDSTONE ARSENAL ALABAMA 35809	DR. WALTER WHARTON
1	U.S. NAVAL ORDNANCE TEST STATION	CODE 4562

	CHINA LAKE	CHIEF, MISSILE
	CALIFORNIA 93557	PROPULSION DIV.

CPIA

1	CHEMICAL PROPULSION INFORMATION AGENCY	P. MARTIN
	APPLIED PHYSICS LABORATORY	
	8621 GEORGIA AVENUE	
	SILVER SPRING, MARYLAND 20910	

INDUSTRY CONTRACTORS

1	AEROJET-GENERAL CORPORATION	L. F. KOHRS
	P. O. BOX 296	
	AZUSA, CALIFORNIA 91703	

1	AEROJET-GENERAL CORPORATION	R. STIFF
	P. O. BOX 1947	
	TECHNICAL LIBRARY, BLDG 2015, DEPT. 2410	
	SACRAMENTO, CALIFORNIA 95809	

1	AERONUTRONIC DIVISION	MR. N. STERN
	PHILCO CORPORATION	
	FORD ROAD	
	NEWPORT BEACH, CALIFORNIA 92663	

1	AEROSPACE CORPORATION	MR. M. J. RUSSI
	2400 EAST EL SEGUNDO BOULEVARD	
	P. O. BOX 95085	
	LOS ANGELES, CALIFORNIA 90045	

1	AIR RESEARCH MFG. CO.	MR. C. S. COE
	9851 SEPULVEDA BLVD	
	LOS ANGELES, CALIF. 90045	

1	ARTHUR D. LITTLE, INC.	E. KARL BASTRESS
	20 ACORN PARK	
	CAMBRIDGE, MASSACHUSETTS 02140	

1	ASTROPOWER LABORATORY	DR. GEORGE MOC
	DOUGLAS AIRCRAFT COMPANY	DIRECTOR, RESEARCH
	2121 PAULARINO	
	NEWPORT BEACH, CALIFORNIA 92663	

1	ASTROSYSTEMS INTERNATIONAL, INC.	A. MENDENHALL
	1275 BLOOMFIELD AVENUE	
	FAIRFIELD, NEW JERSEY 07007	

1	ATLANTIC RESEARCH CORPORATION	A. SCURLOCK
	EDSALL ROAD AND SHIRLEY HIGHWAY	
	ALEXANDRIA, VIRGINIA 22314	

1	BEECH AIRCRAFT CORPORATION BOULDER DIVISION BOX 631 BOULDER, COLORADO 80302	J. H. RODGERS
1	BELL AEROSYSTEMS COMPANY P.O. BOX 1 BUFFALO, NEW YORK 14240	J. FLANAGAN
1	BENDIX SYSTEMS DIVISION BENDIX CORPORATION 3300 PLYMOUTH ROAD ANN ARBOR, MICHIGAN 48105	JOHN M. BRUEGER
1	BOEING COMPANY P. O. BOX 3707 SEATTLE, WASHINGTON 98124	J. D. ALEXANDER
1	MISSILE DIVISION CHRYSLER CORPORATION P. O. BOX 2628 DETROIT, MICHIGAN 48231	JOHN GATES
1	WRIGHT AERONAUTICAL DIVISION CURTISS-WRIGHT CORPORATION WOOD-RIDGE, NEW JERSEY 07075	G. KELLEY
1	MISSILE AND SPACE SYSTEMS DIVISION DOUGLAS AIRCRAFT COMPANY, INC. 3000 OCEAN PARK BOULEVARD SANTA MONICA, CALIF. 90406	R. W. HALLET CHIEF ENGINEER ADVANCED SPACE TECH.
1	AIRCRAFT MISSILES DIVISION FAIRCHILD HILLER CORPORATION HAGERSTOWN, MARYLAND 21740	J. S. KERR
1	GENERAL DYNAMICS CONVAIR DIVISION 5001 KEARNY VILLA ROAD P.O. BOX 1628 SAN DIEGO, CALIF. 92112	E.R. PETERSON V.P., RESEARCH AND ENG.
1	MISSILE AND SPACE SYSTEMS CENTER GENERAL ELECTRIC COMPANY VALLEY FORGE SPACE TECHNOLOGY CENTER P.O. BOX 8555 PHILADELPHIA, PA.	F. MEZGER
1	ADVANCED ENGINE + TECHNOLOGY DEPT. GENERAL ELECTRIC COMPANY CINCINNATI, OHIO 45215	D. SUICHU
1	GRUMMAN AIRCRAFT ENGINEERING CORP. BETHPAGE, LONG ISLAND NEW YORK 11714	JOSEPH GAVIN
1	HONEYWELL, INC. AEROSPACE DIV.	MR. GORDON HARMS

2600 RIDGWAY RD
MINNEAPOLIS, MINN.

| 1 | HUGHES AIRCRAFT CO.
AEROSPACE GROUP
CENTINELA AND TEALE STREETS
CULVER CITY, CALIF. | E.H. MEIER
V.P. AND DIV. MGR.,
RESEARCH AND DEV. DIV. |

| 1 | WALTER KIDDE AND COMPANY, INC.
AEROSPACE OPERATIONS
567 MAIN STREET
BELLEVILLE, NEW JERSEY | MR. R. J. HANVILLE
DIR. OF RESEARCH ENGR. |

| 1 | LING-TEMCO-VOUGHT CORPORATION
ASTRONAUTICS
P. O. BOX 5907
DALLAS, TEXAS 75222 | GARLAND WHISENHUNT |

| 1 | LOCKHEED MISSILES AND SPACE CO.
ATTN-TECHNICAL INFORMATION CENTER
P.O. BOX 504
SUNNYVALE, CALIFORNIA 94088 | Y. C. LEE |

| 1 | LOCKHEED PROPULSION COMPANY
P. O. BOX 111
REDLANDS, CALIFORNIA 92374 | H. L. THACKWELL |

| 1 | THE MARQUARDT CORPORATION
16555 SATICOY STREET
VAN NUYS, CALIF. 91409 | WARREN P. BOARDMAN, JR. |

| 1 | BALTIMORE DIVISION
MARTIN MARIETTA CORPORATION
BALTIMORE, MARYLAND 21203 | JOHN CALATHES (3214) |

| 1 | DENVER DIVISION
MARTIN MARIETTA CORPORATION
P. O. BOX 179
DENVER, COLORADO 80201 | J. D. GOODLETTE (A-241)
A. J. KULLAS |

| 1 | ORLANDO DIVISION
MARTIN MARIETTA CORP.
BOX 5837
ORLANDO, FLORIDA | MR. J. FERM |

| 1 | MCDONNELL AIRCRAFT CORPORATION
P. O. BOX 516
MUNICIPAL AIRPORT
ST. LOUIS, MISSOURI 63166 | R. A. HERZMARK |

| 1 | ROCKET RESEARCH CORPORATION
520 SOUTH PORTLAND STREET
SEATTLE, WASHINGTON 98108 | FOY MCCULLOUGH, JR. |

| 1 | SPACE + INFORMATION SYSTEMS DIVISION
NORTH AMERICAN AVIATION, INC.
12214 LAKEWOOD BLVD
DOWNEY, CALIFORNIA 90241 | H. STORMS |

1	ROCKETDYNE (LIBRARY 586-306) NORTH AMERICAN AVIATION, INC. 6633 CANOGA AVENUE CANOGA PARK, CALIF. 91304	E. B. MONTEATH
1	NORTHROP SPACE LABORATORIES 3401 WEST BROADWAY HAWTHORNE, CALIFORNIA 90250	DR. WILLIAM HOWARD
1	ASTRO-ELECTRONICS DIVISION RADIO CORPORATION OF AMERICA PRINCETON, NEW JERSEY 08540	Y. BRILL
1	REACTION MOTORS DIVISION THIOKOL CHEMICAL CORPORATION DENVILLE, NEW JERSEY 07832	ARTHUR SHERMAN MR. ROBERT GERE
1	REPUBLIC AVIATION CORPORATION FARMINGDALE LONG ISLAND, NEW YORK	DR. WILLIAM O-DONNELL
1	SPACE GENERAL CORPORATION 9200 EAST FLAIR AVENUE EL MONTE, CALIFORNIA 91734	C. E. ROTH
1	STANFORD RESEARCH INSTITUTE 333 RAVENSWOOD AVENUE MENLO PARK, CALIFORNIA 94025	LIONEL DICKINSON
1	TRW SYSTEMS ONE SPACE PARK REDONDO BEACH, CALIF. 90278	MR. D. LEE
1	TAPCO DIVISION TRW, INCORPORATED 23555 EUCLID AVENUE CLEVELAND, OHIO 44117	P. T. ANGELL
1	THIOKOL CHEMICAL CORPORATION HUNTSVILLE DIVISION HUNTSVILLE, ALABAMA 35807	JOHN GOODLOE
1	UNITED TECHNOLOGY CENTER 587 METHILDA AVENUE P. O. BOX 358 SUNNYVALE, CALIFORNIA 94088	B. ADELMAN
1	FLORIDA RESEARCH AND DEVELOPMENT PRATT AND WHITNEY AIRCRAFT UNITED AIRCRAFT CORPORATION P. O. BOX 2691 WEST PALM BEACH, FLORIDA 33402	R.J. COAR
1	VICKERS INC BOX 302 TROY, MICHIGAN	
1	SUNSTRAND AVIATION	MR. R. W. REYNOLDS

2421 11TH STREET
ROCKFORD, ILLINOIS 61101

1   HAMILTON STANDARD DIVISON   MR. R. HATCH
     WINDSOR LOCKS, CONN. 06096
     UNITED AIRCRAFT CORP.